AFOSR-TR- 93 0656

(2)

FINAL REPORT

IONIC AND MOLECULAR ENVIRONMENTS IN HETEROGENEOUS ELECTROCATALYSIS: STUDIES BY RADIOACTIVE LABELING AND LEED/AUGER SPECTROSCOPY

by

ANDRZEJ WIECKOWSKI

Department of Chemistry, University of Illinois, Urbana, IL 61801

for

AIR FORCE OFFICE OF SCIENTIFIC RESEARCH

(AFOSR-89-0368)

for the period of 5/1989 to: 5/1993

REPORT DOCUMENTATION PAGE

Form Approved
OMB No 0704-0188

1. AGENCY USE ONLY (Leave blank)	2. REPORT DATE	3. REPORT TYPE AND DATES COVERED
	July 1993	Final Report 5/1/89 - 4/30/93

4. TITLE AND SUBTITLE
Ionic and Molecular Enviornments in Heterogeneous Electrocatalysis: Studies by Radioactive Labeling and LEED/AUGER Spectroscopy

5. FUNDING NUMBERS
61102F 2303 AS

6. AUTHOR(S)
Andrzej Wieckowski

7. PERFORMING ORGANIZATION NAME(S) AND ADDRESS(ES)
Univ of Illinois
801 South Wright Street
Champaign, IL 61820-6242

8. PERFORMING ORGANIZATION REPORT NUMBER

9. SPONSORING/MONITORING AGENCY NAME(S) AND ADDRESS(ES)
AFOSR/NC
Building 410, Bolling AFB DC
20332-6448

10. SPONSORING/MONITORING AGENCY REPORT NUMBER
AFOSR-89-0368

11. SUPPLEMENTARY NOTES

12a. DISTRIBUTION/AVAILABILITY STATEMENT
APPROVED FOR PUBLIC RELEASE; DISTRIBUTION IS UNLIMITED.

12b. DISTRIBUTION CODE

13. ABSTRACT *(Maximum 200 words)*
See Attached

14. SUBJECT TERMS

15. NUMBER OF PAGES
42

16. PRICE CODE

17. SECURITY CLASSIFICATION OF REPORT	18. SECURITY CLASSIFICATION OF THIS PAGE	19. SECURITY CLASSIFICATION OF ABSTRACT	20. LIMITATION OF ABSTRACT
UNCLASSIFIED	UNCLASSIFIED	UNCLASSIFIED	

13. Adsorption, catalytic activity and metal deposition at the metal/solution interface have been studied in a coordinated fashion by radiochemistry, ultra-high vacuum spectroscopies of surface science and electrochemistry. The metal part of the interface was usually a single-crystal of platinum, rhodium or gold, or an ultra-thin metallic film of either cadmium, copper or silver obtained via underpotential deposition processes. The adsorbates predominantly included bisulfate, perchlorate, phosphate, acetic acid and urea. The integrative feature of the adsorbates was their capacity of a reversible adsorption on the platinum electrode. The molecule with which the catalytic rates have been measured was methanol in perchlorate, bisulfate and phosphate solutions. These studies have focused on (i) effects of anions on the catalytic oxidation of methanol on platinum single crystal electrodes, (ii) surface chemistry of the studied adsorbates on the clean and admetal covered electrodes, (iii) surface studies of the solid/liquid CO (as the most probable methanol chemisorption product), and (iv) phase transitions of urea induced by lateral adsorbate-adsorbate interactions. Two methods for in situ and ex situ electrode characterization, namely the radioactive labeling and the ultra-high vacuum-electrochemistry, have been used and advancements in their performance, or new areas of applications, have been reported. With the well-ordered single crystal electrodes chosen for this program, we have observed a phase transition character of some of the studied adsorption/desorption processes. Theoretical analysis of an exemplary phase transition process has been conducted for urea adsorption on the Pt(100) electrode. The conclusions that we are reporting herein would be difficult to arrive at, or made quantitative, with polycrystalline surfaces that do not have the regular atomic periodicity and a long range crystallographic order. We have also demonstrated that the well-ordered, surface phases of the reversible adsorbates are accessible to low energy electron diffraction (LEED) investigations. The structural data thus obtained are present in this document.

In the domain of heterogeneous electrocatalysis, we have found that the rates of catalytic electrooxidation of methanol on platinum obtained by chronoamperometry increase by a factor of 50 when perchlorate rather than phosphate solution is used. That is, specific adsorption of anions significantly retards methanol oxidation. Utilizing the same chronoamperometric approach we have found the Pt(110) electrode is much more catalytic in the methanol oxidation process thatn is the Pt(111) one. While such effects had qualitatively been known before, owing to earlier voltammetric studies by others, our investigations determined the magnitude of these effects on the quantitative level. We have also produced many new pieces of surface information on the solid/liquid CO -- as the main poison in oxidative heterogeneous electrocatalysis of methanol -- by the use of ultra-high vacuum techniques.

FINAL REPORT

IONIC AND MOLECULAR ENVIRONMENTS IN HETEROGENEOUS ELECTROCATALYSIS: STUDIES BY RADIOACTIVE LABELING AND LEED/AUGER SPECTROSCOPY

by

ANDRZEJ WIECKOWSKI

Department of Chemistry, University of Illinois, Urbana, IL 61801

for

AIR FORCE OFFICE OF SCIENTIFIC RESEARCH

(AFOSR-89-0368)

for the period of 5/1989 to: 5/1993

TABLE OF CONTENT

I. ABSTRACT

Adsorption, catalytic activity and metal deposition at the metal/solution interface have been studied in **a coordinated fashion** by radiochemistry, ultra-high vacuum spectroscopies of surface science and electrochemistry. The metal part of the interface was usually a single-crystal of platinum, rhodium or gold, or an ultra-thin metallic film of either cadmium, copper or silver obtained via underpotential deposition processes. The adsorbates predominantly included bisulfate, perchlorate, phosphate, acetic acid and urea. The **integrative feature** of the adsorbates was their capacity of a reversible adsorption on the platinum electrode. The molecule with which the catalytic rates have been measured was methanol in perchlorate, bisulfate and phosphate solutions. These studies have focused on (i) effects of anions on the catalytic oxidation of methanol on platinum single crystal electrodes, (ii) surface chemistry of the studied adsorbates on the clean and admetal covered electrodes, (iii) surface studies of the solid/liquid CO (as the most probable methanol chemisorption product), and (iv) phase transitions of urea induced by lateral adsorbate-adsorbate interactions. Two methods for in situ and ex situ electrode characterization, namely the radioactive labeling and the ultra-high vacuum-electrochemistry, have been used and advancements in their performance, or new areas of applications, have been reported. With the well-ordered single crystal electrodes chosen for this program, we have observed a phase transition character of some of the studied adsorption/desorption processes. Theoretical analysis of an exemplary phase transition process has been conducted for urea adsorption on the Pt(100) electrode. The conclusions that we are reporting herein would be difficult to arrive at, or made quantitative, with polycrystalline surfaces that do not have the regular atomic periodicity and a long range crystallographic order. We have also demonstrated that the well-ordered, surface phases of the reversible adsorbates are accessible to low energy electron diffraction (LEED) investigations. The structural data thus obtained are present in this document.

In the domain of heterogeneous electrocatalysis, we have found that the rates of catalytic electrooxidation of methanol on platinum obtained by chronoamperometry increase by a factor of 50 when perchlorate rather than phosphate solution is used. That is, specific adsorption of anions significantly retards methanol oxidation. Utilizing the same chronoamperometric approach we have found the Pt(110) electrode is much more catalytic in the methanol oxidation process than is the Pt(111) one. While such effects had qualitatively been known before, owing to earlier voltammetric studies by others, our investigations determined the magnitude of these effects on the **quantitative** level. We have also produced many new pieces of surface information on the solid/liquid CO -- as the main poison in oxidative heterogeneous electrocatalysis of methanol -- by the use of ultra-high vacuum techniques. These very recent accomplishments in the field of electrocatalysis create a framework for a new proposal for which we will be seeking support by AFOSR. We are submitting the new proposal as a separate document.

II. AFOSR GRANT OVERVIEW

II.1. General statement

The P. I. has been supported by the Air Force Office of Scientific Research since 1989. As stated in the original proposal, the focus of this research has been the investigation of the structure of the solid/liquid interface containing reversible adsorbates: bisulfate, phosphate, acetic acid and urea. The key part of this program was to document the connection between heterogeneous electrocatalysis and the structure of the solid/liquid interface (as the effective part of the electrochemical environment in the electrode reactivity). We have also given much attention to interactions of the reversibly adsorbed species with ultra-thin metallic films of cadmium copper, silver, electrodeposited on platinum and gold. We have extended our exploration to interfacial dynamics with which the electrical double layer responded to the chemical and electrical perturbation. A parallel aim has been to develop new experimental and theoretical approaches for studying electrode adsorption. By using these new techniques and the well-defined electrodes we have performed electrochemical and physical measurements of the surface-related electrode processes with high reproducibility and resolution.

A manifestation of the P. I. laboratory contribution to catalysis has been the recently obtained **structure/function** relationship in the electrooxidation of methanol. Using fast current transient measurements we have found that the specific adsorption of anions significantly retards methanol oxidation, (by a factor of approximately 50 in an extreme case). Overall, by varying surface crystallography of the electrodes, and their anionic compositions, we have been able to tune the methanol oxidation rates by three orders of magnitudes at a constant electrode potential and bulk concentration of methanol. As mentioned above, while such effects had been known before, their magnitude, and the quantitative treatment, have become possible due to our recent chronoamperometric insight.

Likewise in the domain of catalysis, we have provided evidence that formation of ultra-thin metal deposits via electrochemistry (underpotential deposition processes) is associated with an excessive anion adsorption. Since the anions inhibit methanol electrolysis, the catalytic enhancement effects by the metal adatoms, whenever observed, may be counteracted by the inhibition through the anion adsorption. The proper choice of the anionic electrochemical environment of the catalysis may amplify the enhancement. This observation should be taken into account in modeling more advanced, multicomponent electrocatalysts, and electrolytic media, in future catalytic electrochemical technologies.

Our most recent study has focused on the voltammetry of platinum electrodes in solutions containing urea. In a collaboration with Professor P. A. Rikvold, FSU, we have developed a lattice-gas model of urea adsorption on the Pt(100) electrode, and demonstrated that the simulated results agree well with those of the experiments. We provide evidence that a phase transition occurs between a c(4x2) phase of urea a (1x1) monolayer of hydrogen phase, and the effective lateral interaction energies have been obtained. This work demonstrates how the unique electrochemical properties and resolution of single crystal electrodes contribute to progress in understanding of surface phenomena in electrochemistry.

II.2. The list of specific accomplishments:

The accomplishments resulting from the four year research can be summarized as follows (in a roughly chronological order):

- progress in the methodology of surface science: radiochemistry and UHV-electrochemistry techniques [1-8,12,14,19,24,30,34,37];
- characterization of electrode adsorption on single crystal electrodes by the use of radioactive labeling method [2-3,6,7,10,11-14,16,17,19-21,24,26,27,29,32,33];
- first successful preparation and characterization of single crystal electrodes of rhodium [4,5,13]. Evidence for perchlorate reduction on rhodium [9,18];
- LEED/Auger analysis of carbon monoxide adsorbed in aqueous solutions (as a well-known catalyst poison in methanol fuel cell applications) [4,8,23,25,30];
- measurements of adsorption of reversible electroadsorbates via the UHV techniques [18,26,33,35,37-39];
- correlating anion surface chemistry with the processes of ultra-thin electrodeposit formation on single crystal electrodes [10,17,20,21,24,27,38];
- phase transitions of urea on the Pt(100) electrode induced by lateral adsorbate-adsorbate interactions [15,22,33,39];
- quantifying anion effects in catalytic oxidation of methanol on platinum single crystal (well-ordered) electrodes [36,40,41];

The work completed to date has been divided into several distinct but interrelated projects that are summarized below.

III. RESULTS from AFOSR SUPPORT

III. 1. Effects of surface anions on methanol oxidation kinetics on platinum single crystal electrodes: study by chronoamperometry.

We have completed a quantitative determination of an **anionic effect** in the catalytic decomposition of methanol on platinum single crystal electrodes [36,40,41]. The anions were those present in sulfuric acid and phosphoric acid solutions, frequently dissolved in 0.1 M of perchloric acid. For simplicity, the anions are named perchlorate, bisulfate and phosphate. With reference to perchlorate, which is known not to interact strongly with surfaces of metal electrodes (unless is reduced to chloride, see below), bisulfate and phosphate are the effectively adsorbing anions. The rate measurements

were conducted using **chronoamperometry** and a multiple potential pulsing electrode pretreatment developed by us for the catalytic solid/liquid investigations. Earlier work by cyclic voltammetry carried out by other investigators -- while gave a good starting point for the chronoamperometric study -- had been unable to provide a quantitative insight into methanol oxidation rates. This is because of a persistent inability of the voltammetry to decouple methanol self-inhibition (to surface CO) from its oxidation (to dissolved CO_2). The combined application of the fast current-time transients (the oxidation current was measured on a **millisecond** time scale) and the **well-defined electrodes**, enabled us to circumvent these adverse effects.

Obtaining consistent and reproducible results required regeneration of the surface order before every individual current-time measurement. With such prepared electrodes, Figure 1, and with the experimental chronoamperometric procedure developed, we may have, for the first time, the **correct instantaneous values of methanol oxidation currents**. We have used these instantaneous (zero-time) currents as the kinetic variable representing the rate of the catalytic decomposition of methanol on the platinum surface in the absence of methanol self-poisoning. (In view of the *rapid* delivery of methanol to the surface under the chosen working conditions, as referenced to the amount of the current generated, the current decay gives the rate of surface poisoning by CO). The results are shown in Figure 2 where the instantaneous current and related turnovers are plotted vs. the electrode potential. It is shown that the oxidation rates change by three orders of magnitudes between the extreme cases has also been observed. With the Pt(110) electrode in perchloric acid solution, the oxidation current taken at 0.20 V[1], is 156 $mA \cdot cm^{-2}$. As reiterated in Table 1, the highest oxidation current corresponds to a turnover of **162.5 molecules (Pt site)$^{-1} \cdot s^{-1}$**, Table 1. **This is an extremely high turnover**, in fact, much

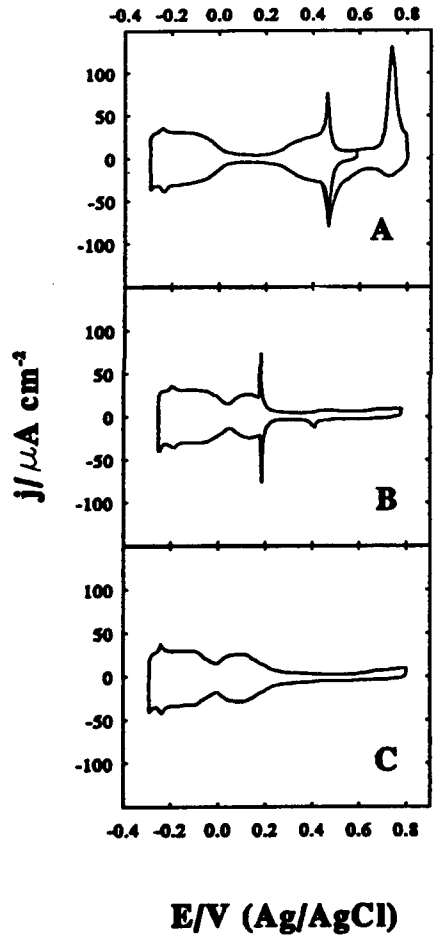

Figure 1. Cyclic voltammetric profile of the Pt(111) electrode in A) 0.1 M $HClO_4$, B) 0.1 M H_2SO_4 and C) 0.1 M H_3PO_4. (Example of the quality of the electrode used for this project).

[1]**Unless otherwise indicated the potentials given in this report are referred to the Ag/AgCl reference electrode in sodium chloride solution of 1.0 M.**

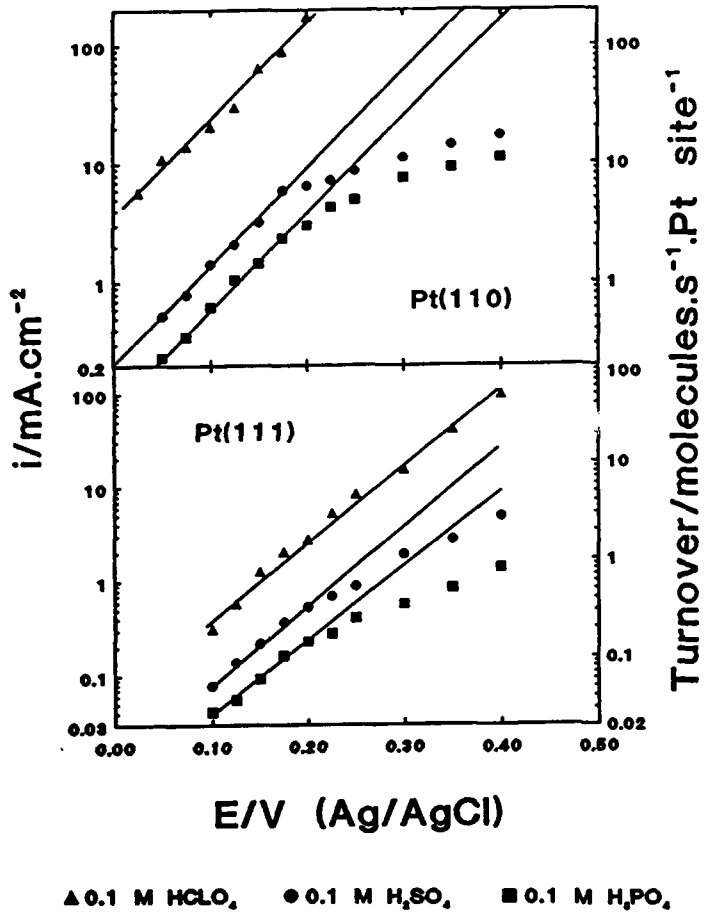

Figure 2. Butler-Volmer kinetics (and deviations from the straight B-V lines) for methanol oxidation in the three supporting electrolytes studied for the Pt(110) and Pt(111) electrodes.

higher than previously believed [42]. Breaking up the total effect into individual substrate and environment contributions shows that the surface geometry and the anionic effects are roughly comparable (cf. data in Figure 2). That is, the increase in the catalytic oxidation current by a factor of 50 may be achieved by a proper choice of the electrolyte anion alone. This shows that **the inhibiting anion-platinum interactions are as important in determining the rates of methanol oxidation as is the proper surface geometry of the Pt catalyst.**

The key result of this work is a **deviation** of the experimental current-potential plot from the line predicted by **Butler-Volmer** kinetics, with the $n_\alpha\alpha = 0.5$, Figure 3 [36]. With the Pt(111) electrode, the beginning of such a deviation coincides [26] with the end of the voltammetric splitting in the conventional double layer range of the electrode potentials (ref. 16 and references therein). Since the end of the splitting corresponds to a completion of the monolayer of the anionic adsorbates, we may conclude that the slowdown of the oxidation rates begins on the surface already covered by the anions at the saturation coverage. We found that the catalytic oxidation rates of formic acid and formaldehyde at 0.20 V gave the current that was two and ten times higher than that with methanol, respectively. Assuming that the replacement rate of platinum bisulfate by methanol, formic acid and formaldehyde is similar -- because of the similar molecular characteristics -- we have an evidence that this decelerating effect is not due to a simple blocking of the surface sites by the bisulfate. This observation confirms earlier radiochemical evidence that bisulfate adsorption is reversible and that the rate of exchange of the surface and the bulk anion is fast [16]. Therefore, we may assume that the oxidation of methanol occurs after the efficient anion/methanol replacement on the

Table 1. Current densities and Tafel slopes obtained in three supporting electrolytes with 0.2 M CH_3OH on Pt(110)

	Tafel slope mV/dec.	$i_{E=0.2\ V}$ /mA cm^{-2}	i_{cv} /mA cm^{-2}
0.1 M $HClO_4$	121	156	32.4
0.1 M H_2SO_4	123	4.47	14.9
0.1 M H_3PO_4	123	3.00	11.1

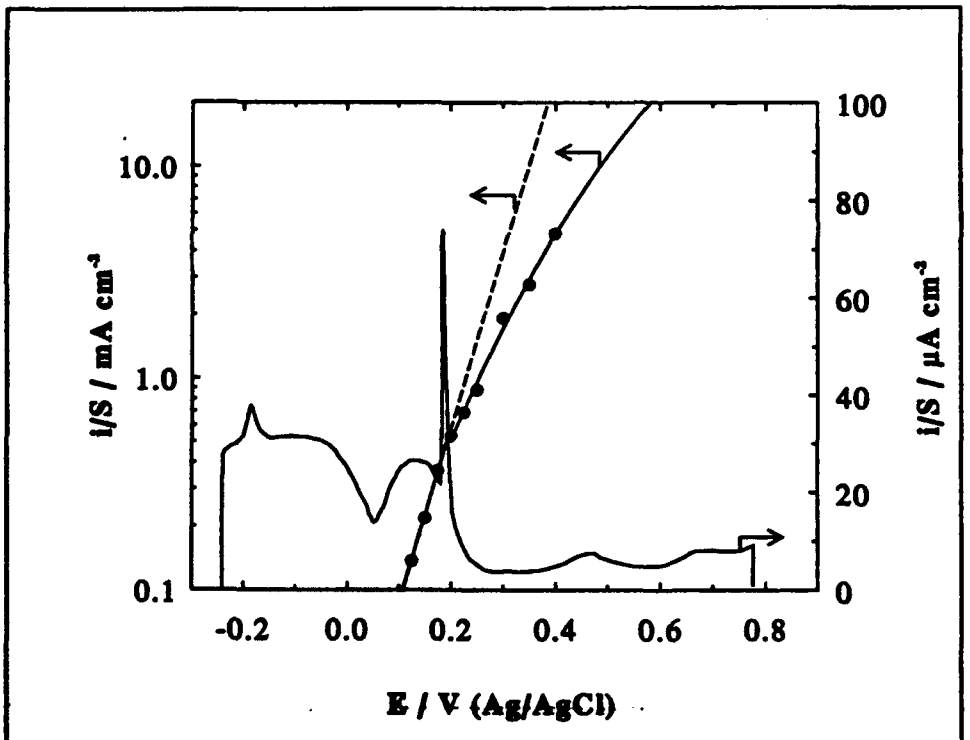

Figure 3. Semi-log plot of instantaneous current (circles) vs. electrode potential obtained for methanol oxidation in 10^{-1} M H_2SO_4 and 0.2 M CH_3OH. The solid curve is the least-squares plot obtained for $\lambda = 0.90$ eV and $v\sigma = 1.8 \times 10^{-2}$. $(s\text{-}eV)^{-1}$ [36]. The straight line represents the Butler-Volmer kinetics. The voltammetric curve for the Pt(111) in clean 0.1 M H_2SO_4 is also shown.

clean metal sites. However, following the replacement, the surface site(s) occupied by the methanol molecule are surrounded by the adsorbed anions. The situation closely resembles the one encountered by a redox center in a chemical or electrochemical redox. Therefore, we conclude that we have identified a strong electronic effect in methanol oxidation kinetics exerted by co-adsorbed surface surface-anion-ligands. The nature of this effect will be actively investigated in the P. I. laboratory.

*While the structural catalytic electrochemistry has successfully been developed over the last decade, the measurements of rates with single crystal electrodes of platinum metals are in their infancy. Our work has added to this area, and provided quantitative information on the crystallographic and anionic effects in heterogeneous electrocatalysis. The **fast turnovers** that we have identified in this project show that the fabrication of a potent methanol oxidation catalysts is more feasible that previously believed. However, the lingering problem with the CO poisoning remains [36,40,41]. We conclude that advancements in electrochemical methodology and in theory of the electrode catalysis are needed to learn how to significantly suppress the CO poisoning effect versus methanol reactivity. This issue will be addresses in the new AFOSR proposal that is under preparation.*

III.2. Surface Chemistry of Solution Anions. Clean Surfaces.

As we have demonstrated above, the proper selection of solution anions, also present on the electrode surface, is essential in performing efficient methanol electrocatalysis. However, there are other reasons to be interested in surface chemistry of anions. Perchlorate, bisulfate and phosphate interact with the surface with a disparate strength. This diversity of the surface forces is reflected by the way these anions modify the voltammetry of metal, especially single crystal electrodes. The anions also affect the structure of the underpotentially deposited metal overlayers and, due to their charge, alter distribution of the electric field at the solid/solution interface. **Therefore, the understanding of anion's surface chemistry is needed to optimize rates of heterogeneous electrocatalytic processes, to develop realistic theories of the electrochemical interface, and to assess the performance of the electroanalytical methods.** The molecular-level explanation of some of these effects has been sought in this research.

Below, summarized will be the results of characterization of adsorbed bisulfate on well-defined single crystal electrodes of platinum, rhodium and gold, and on ultra-thin metallic films deposited on the corresponding single crystal substrates. We will also reveal interdependencies between surface packing by metal adatoms and by the anions. Based upon the analysis of adsorption on the clean substrates, and on the thin metallic deposits, we will provide information on the weak anion chemisorption, and on the nature of the metal adlayers with which the anions interact.

To fulfill research requirements of this program, we have developed a radiochemical methodology to study adsorption processes in situ and was integrated (on the interpretation level) with the ex situ methods of surface analysis. In the latter case, after adsorption under potential control, the adsorbate-covered working electrode is emersed and transferred to the UHV without exposure to the atmosphere. The spectroscopic techniques applied include the Low-Energy Electron Diffraction (LEED) for the surface crystallographic insight, the Auger Electron Spectroscopy (AES) for coverage measurements, and the X-ray photoelectron spectroscopy for probing the core electronic levels of metallic adsorbates. Finally, standard, high-precision electrochemical

instrumentation, in particular cyclic voltammetry, has been used for this program. The progress in the methodology of this research have been systematically reported, including Interim Reports that have been submitted for AFOSR during the contract period [1].

III.2.1. Radiochemistry and voltammetry.

The studies have included correlated measurements of bisulfate adsorption by radiochemistry and voltammetry on several single crystal electrodes: Pt(111), Pt(100), Au(111) and Rh(111) [6,13,16,32,35,36,38]. The isotherms (surface concentration versus the electrode potential data) are shown in a combined Figure 4. The companion figure with the relevant voltammograms is Figure 5. The main observations may be summarized as follows:

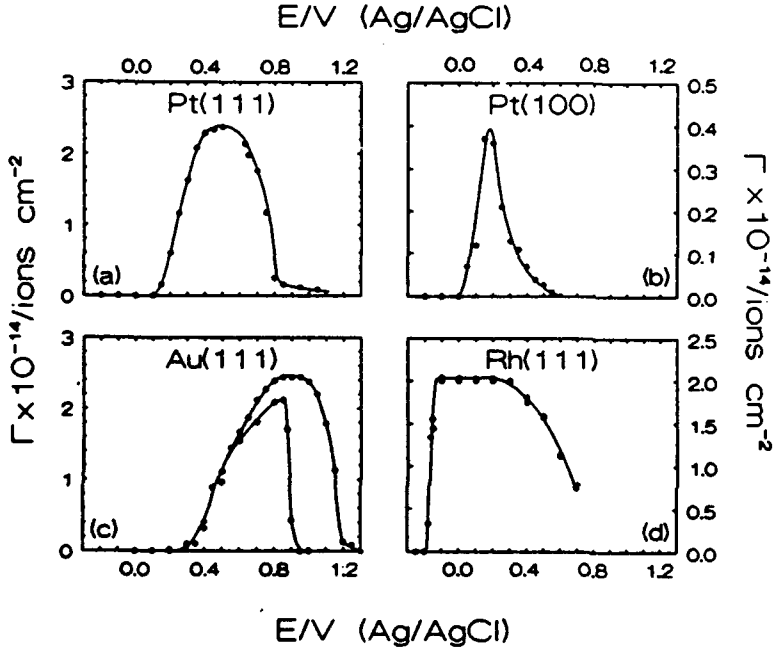

Figure 4. Potential dependence of (bi)sulfate adsorption in 0.1M perchloric acid with sulfuric acid in the millimolar concentration range on: (a) - Pt(1111), (b) - Pt(100), (c) - Au(111) and (d) - Rh(111) electrodes.

- bisulfate anion is adsorbed in the double layer range of the electrode potentials;
- except for the Rh(111) electrode [13], bisulfate desorbs from the surface of the studied metals along with the progress in surface oxidation;
- the electrode potential bias that determines the negative potential adsorption threshold depends on the presence or absence of adsorbed hydrogen, and on the adsorbed hydrogen energetics on the studied surfaces. (i) On Pt(111), the adsorption may be related to high-energy-hydrogen adsorption [16]; (ii) on Pt(100), the bisulfate adsorption is weak and, under the reported experimental conditions, it barely affecting the adsorbed hydrogen (iii) on Rh(111), bisulfate is adsorbed at the expense of a conventional hydrogen compression; (iv) on Au(111), since there is no hydrogen adsorption, the onset of bisulfate adsorption is determined by the position of the of the Au(111) in the studied medium [24].

Highlighting some key observations we notice that bisulfate surface concentration is very low: 4.0x1013 ions per cm-2 (0.03 ML), Figure 6. To account for bisulfate

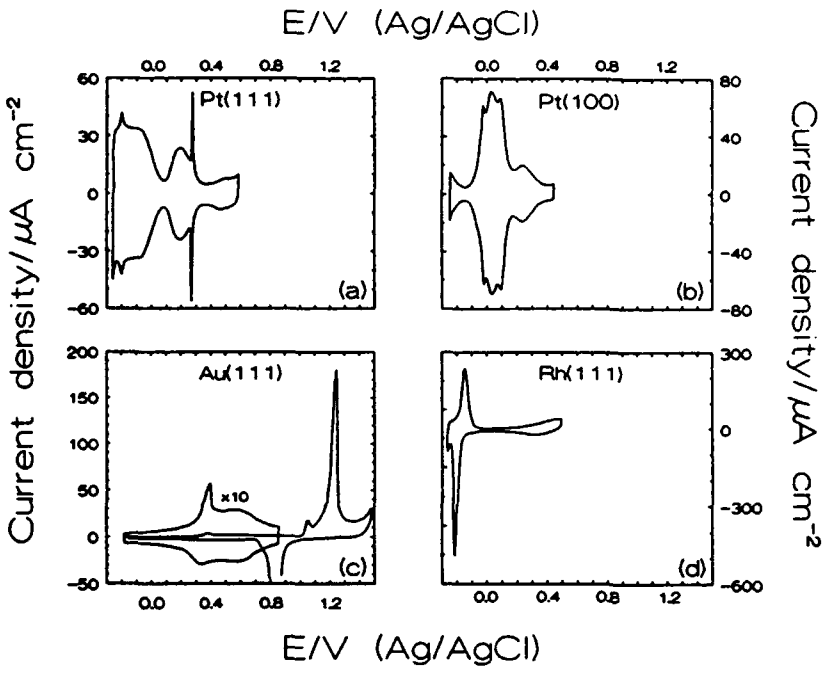

Figure 5. Cyclic voltammograms of: (a) - Pt(111), (b) - Pt(100), (c) - Au(111) and (d) - Rh(111) electrodes in 0.1M perchloric acid with sulfuric acid in the millimolar concentration range. Scan rate 50 $mV \cdot s^{-1}$.

desorption with increasing positive charge of the electrode, well before platinum oxidation occurs, one needs to assume that bisulfate is forced out from the surface by a competitive adsorbate. The key to understanding of the desorption process is the nature of the positive and negative maxima observed at 0.25 V in the current-potential graphs, Figures 6. We propose that some form of water discharge accounts for the current-potential peaks at 0.25 V. Namely, at $E > 0.15$ V:

$$H_2O_{sln} \rightarrow H_2O_{ads} \quad (1)$$

$$H_2O_{ads} \rightarrow H_2O_{ads}^{\delta+} + \delta e^- \quad (2)$$

where the scheme 2 stands for a partial discharge of a surface water molecule. If so, adsorption of the $H_2O_{ads}^{\delta+}$ species accounts for the forced bisulfate desorption. On the other hand, these water-derived-species are the most likely precursors of the full surface oxidation of platinum, which begins at 0.60 V on the potential scale in use.

Adsorption of bisulfate on the Pt(111) and Au(111) electrodes represents a very interesting case for a surface electrochemist [1[illegible],16,19,32,35,38]. This is because there is a clear voltammetric feature in the double layer region -- not masked by the hydrogen adsorption current -- that can be related to bisulfate adsorption, and the net charge associated with the adsorption can be measured, Figures 5a and 5c. Since, in both cases studied the number of electrons formally exchanged per one adsorbed anion is close to two, one may conclude that the measured charge is due to the divalent sulfate adsorption. This is undoubtedly true on the Au(111) surface since no alternative explanation can be provided: there in no hydrogen adsorption on gold. Such an alternative possibility exists on the Pt(111) where formation of a high-energy-hydrogen has been not only considered,

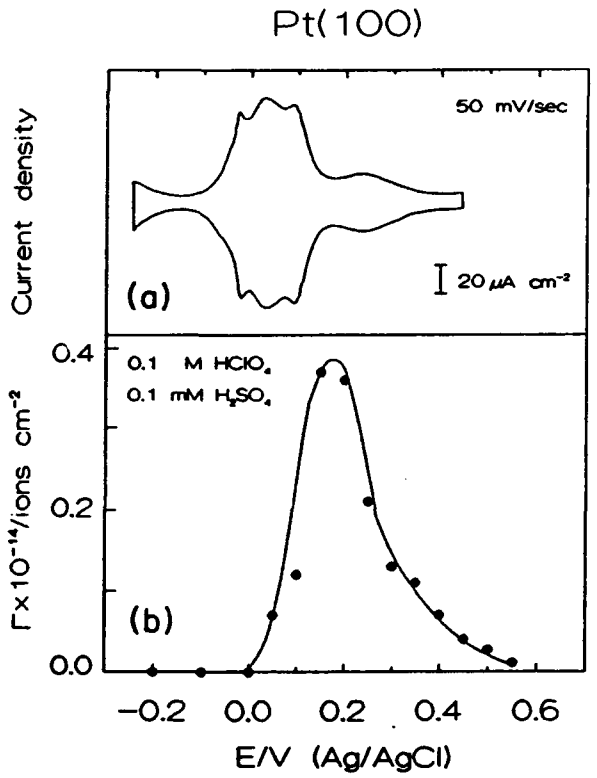

Figure 6. (a) Cyclic voltammogram of Pt(100) in 0.1M $HClO_4$ + 10^{-4}M H_2SO_4. Scan rate 50 mV·s^{-1}. (b) Potential dependence of (bi)sulfate adsorption.

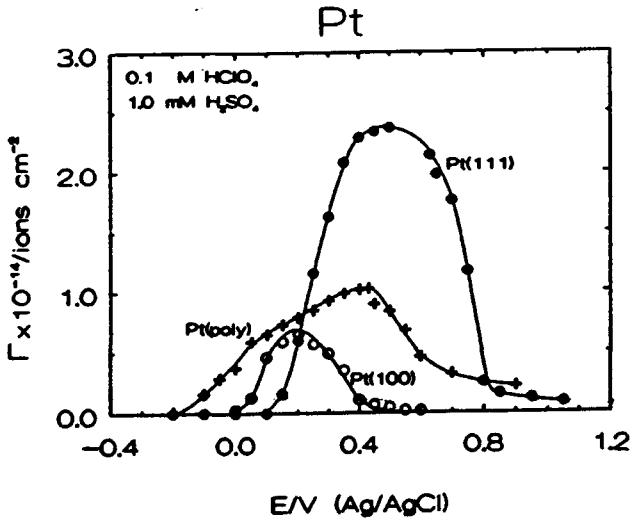

Figure 7. Potential dependence of (bi)sulfate adsorption on: (•) Pt(111), (o) Pt(100) and (+) Pt(poly) electrodes. The data were obtained on 0.1M $HClO_4$ + 10^{-3}M H_2SO_4 solution.

but also strongly indicated by SHG and AC impedance methods (see ref. 16 and references therein). Therefore, the voltammetric current observed with the two metals may be of a different origin. This shows that the explanation of some segments of the voltammetric profile of the Pt(111) electrode in aqueous electrolytes is still not sufficiently advanced. The search for a conclusive solution to the indicated dilemma should probably be postponed until new methods of surface imaging, like surface NMR, with its high sensitivity to protons, are available [43].

To conclude, we reconfigure the data pointing at the single crystal specificity of bisulfate adsorption on platinum, Figure 7. It is seen that the coverage of bisulfate on the Pt(100) electrode is less than one third of the coverage found on the Pt(111) surface (under identical experimental conditions). The behavior of a polycrystalline Pt electrode, also shown in this figure, gives an indication of a superposition of the adsorbates which have their individual Γ vs. E characteristics associated with the different crystallographic facets on the surface. If this assertion is correct, the maximum at 0.50 V obtained with the Pt(100) surface, Figure 7, may be assigned to the Γ vs. E peak on the ordered Pt(111) plane (Figure 2, filled circles). However, it is unlikely that the contribution from the Pt(100) plane gives rise to the discontinuity in the Γ vs. E slope on Pt(poly) at 0.05 V, Figure 7. Bisulfate adsorption below 0.05 V is probably due to the HSO_4^- adsorption

on some other facets than the (100) or (111) one, most probably on (110). *This comparative analysis represents one of the key results of this project.*

III.2.2 Ultra-high vacuum studies of bisulfate adsorption [26,37,38].

The surfaces have been prepared in the UHV using standard procedures. Once the appropriate surface characteristics of the clean surfaces had been obtained, the electrode was transferred to a bisulfate-containing solution for voltammetric characterization and bisulfate adsorption. The Perkin Elmer LEED optics and electronics were used for the LEED measurements in a kinematic approximation. After emersion from solution at the electrode potential of a bisulfate adsorption maximum, the Pt(111)($\sqrt{3}$ x $\sqrt{3}$) structure was found in a broad range of bulk concentration of the acid. The representative LEED patterns are shown in Figure 8. The sharpness of the LEED spots also increases with the increase in bisulfate packing on the electrode surface. That the "$\sqrt{3}$" surface structure is associated with bisulfate adsorption is documented by the Auger electron spectroscopy analysis, Figure 9. After removing the beam damage effects, that is, using only the AES data after an extrapolation to zero time [18,35,38], we have found that the sulfur and oxygen signals appear in proportions corresponding to the S:O stoichiometry in the HSO_4^- (or SO_4^{2-}) adsorbate (1:4). The fact that the LEED pattern (and corresponding bisulfate surface structure) is observed in a broad surface packing range demonstrates that the surface anions, when exposed to the ultra-high vacuum environment, are organized in two-dimensional ($\sqrt{3}$ x $\sqrt{3}$) domains, which size increases with the increase in the sulfuric acid bulk concentration.

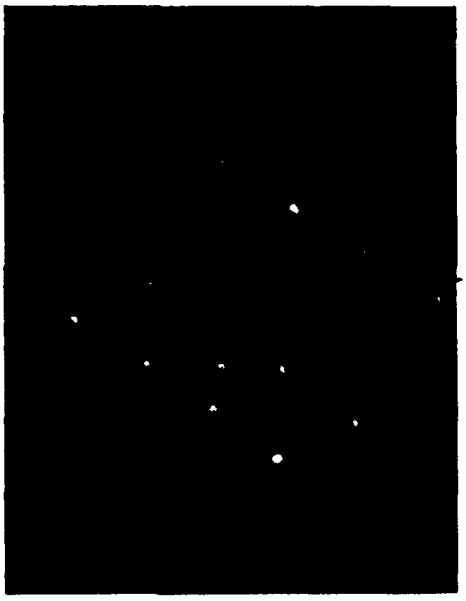

Figure 8. Pt(111)($\sqrt{3}$x$\sqrt{3}$)R30 LEED pattern of bisulfate on the Pt(111) electrode at beam energy of 103 eV.

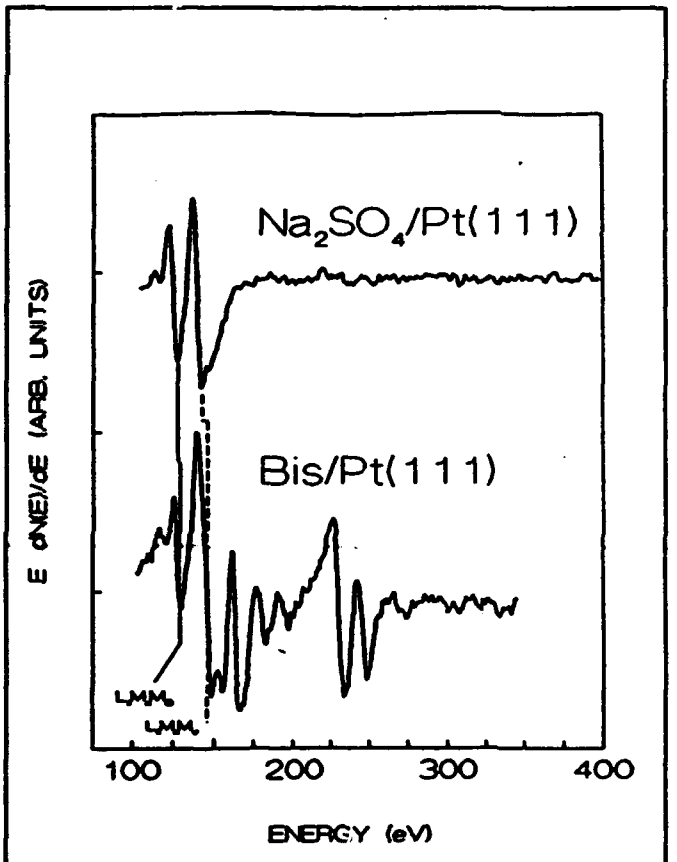

Figure 9. The Auger electron spectra of sulfur in a thick layer of Na_2SO_4 and in bisulfate adsorbed on the Pt(111) electrode in $5x10^{-4}$M H_2SO_4.

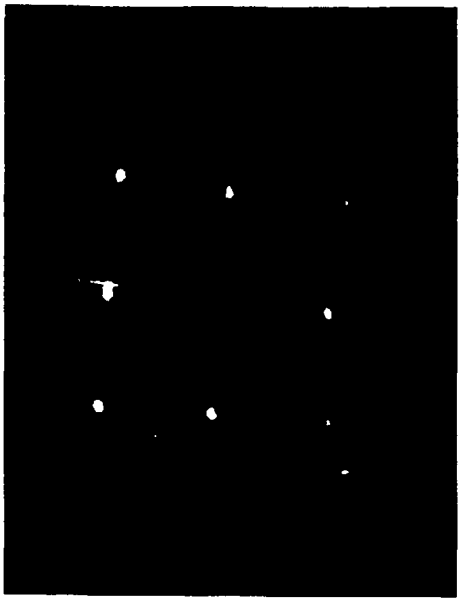

Figure 10. Unreconstructed Pt(100) electrode after emersion from bisulfate containing solution at bisulfate adsorption maximum.

Using Auger electron spectroscopy we have confirmed the bisulfate adsorption on the Pt(100) electrode, originally found by radiochemistry (see ref. 26 and references therein). The LEED pattern of the unreconstructed Pt(100) surface obtained after the electrode emersion to vacuum is shown in Figure 10. The main effect of the immersion is the reconstruction deletion. Contrary to the adsorption on Pt(111), bisulfate does not create an adlattice on the Pt(100) surface. This is a very interesting observation that can be accounted for by noticing that the symmetry of the three bisulfate oxygens fits very well to the symmetry of the hexagonal (111) surface, but not to the square (100) surface. The proper surface-molecule geometric match creates an ordered structure; the poor - or unconfined - does not. These findings show that the adsorption of the reversibly adsorbed species can be seen in terms of a surface pattern recognition mechanism.

After sulfate (SO_4^{2-}) adsorption on Au(111) no clear LEED structure was found (a very faint ($\sqrt{3}$ x $\sqrt{3}$) was sometimes noticed) [38].

The comparison of the data from the chapters III.2.1 and III.2.2, and the discussion in refs. 6,13,16,33,36,37,39 *shows that the adsorption strength of bisulfate on the (111) and (100) crystallographic planes of the studied metals decreases in the following order: Rh(111) > Rh(100) > Pt(111) ≈ Au(111) > Pt(100). We have also documented [24] that the (bi)sulfate interactions with the studied metal electrodes is not purely electrostatic, there is chemical bonding component that decreases in significance in the series: phosphate > bisulfate > perchlorate.*

III.2.3. Perchlorate reduction on rhodium single crystal electrodes

In contrast to the data discussed above, this chapter refers to **a strong anion-surface interactions**. Namely, we will report results of electrochemical and vacuum measurements of the rhodium electrodes in perchloric acid media that indicate **perchlorate reduction** reaction [9,18]. The data analysis shows that the Rh(100) face displays the highest catalytic activity. The reduction is indicated by the voltammetric splitting of electric current associated with the hydrogen adsorption process, Figure 11, for the Rh(100), Rh(111) and polycrystalline rhodium electrodes. (Solution composition is given in the figures.) It is seen that the voltammetric splitting in the hydrogen range, obtained in perchloric acid with the three Rh surfaces studied, is different from those obtained in hydrofluoric acid. Since the splitting is characteristic of the perchlorate

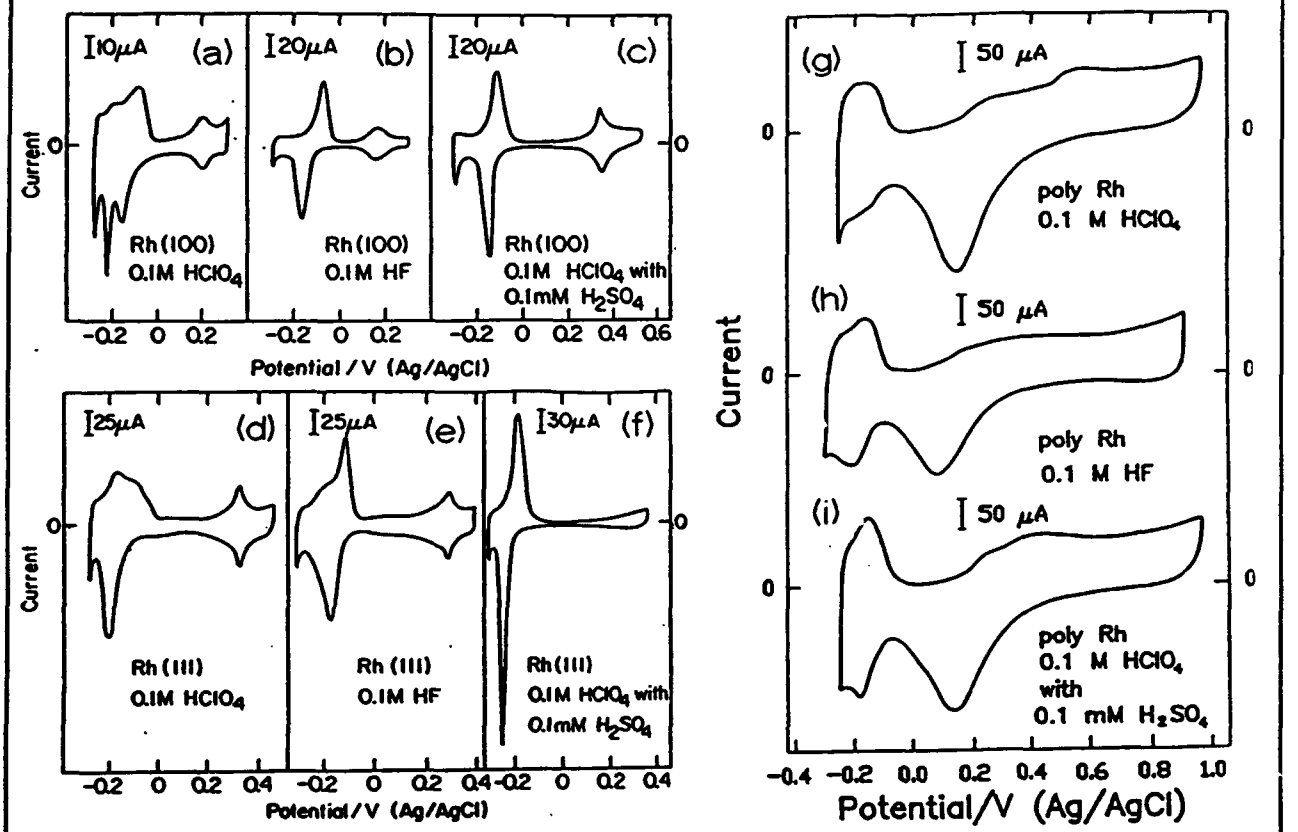

Figure 11. Voltammetry of the Rh(100), Rh(111) and Rh(poly) electrodes in three supporting electrolytes indicating perchlorate reduction (see text). Scan rate 50 $mV \cdot s^{-1}$.

reduction [9,18], this shows that the reduction is characteristic of all the rhodium surfaces. The proposed sequence of events to account for the splitting is: (i) a perchlorate reduction to chloride with the rate maximum at the negative end of the double layer potential range of rhodium, (ii) the chloride adsorption which prevented efficient perchlorate reduction under steady-state conditions, and (iii) surface chloride replacement by adsorbed hydrogen in the hydrogen range of the electrode potentials. Using the Rh(100) electrode, and ultra-high vacuum measurements, we have also provided a direct evidence that chloride resides on the surface after emersion to vacuum [18].

We have carried out the following experiment in order to develop a quantitative grasp of the perchlorate reduction rates. It began with the rhodium surfaces covered by chemisorbed carbon monoxide. Before the measurements of the reduction current, a protective layer of surface CO was voltammetrically stripped-off the surface and the chloride-free rhodium sites were exposed to solution, Figure 12. The peaks observed on the positive-going scan at about 0.4 V for the three surfaces are due to the surface CO stripping. On the reverse run, the observed increase in the negative current at 0.05 V is due to perchlorate reduction, and the current decline below -0.05 V is due to chloride adsorption. Further work has shown that the peak amplitude decreases in the order:

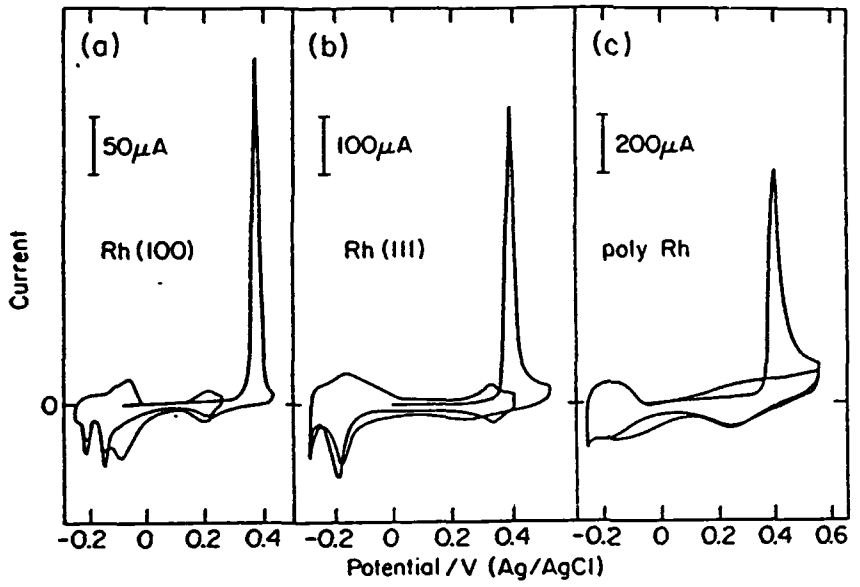

Figure 12. Electrooxidation of a monolayer of carbon monoxide adsorbed on rhodium electrodes in CO-saturated 0.1 M $HClO_4$ solution. Scan rate: 50mV·s^{-1}.

(100), (poly), (111). (For corresponding AES and LEED data of the most active Rh(100) surface, see ref. 18). We therefore conclude that the reduction rate measured under the voltammetric transient conditions falls into the same order.

We have also studied temperature effects in the perchlorate reduction with the Rh(100), Rh(111) and Rh(poly) electrodes [18]. It appears that while the reaction turnovers taken at several temperatures for the Rh(100) and Rh(poly) electrodes are similar that for the Rh(111) electrode is much lower. Therefore, the perchlorate reduction rate changes in the order of Rh(100) > Rh(poly) > Rh(111) (in contrast to the order of Rh(100) > Rh(poly) > Rh(111) obtained under transient conditions). The apparent activation energies are 41 kJ·$mole^{-1}$ for Rh(100) and Rh(poly), and 18 kJ·$mole^{-1}$ for Rh(111). Both values are low, especially that for the Rh(111) electrode, and are below typical values for a catalytic bond splitting of inorganic anions (or molecules) at the solid/liquid interface. We may tentatively account for our observation by assuming that the reduction current is controlled by the availability of surface catalytic sites. This availability is determined, in turn, by the coverage by chloride.

The catalytic specificity observed in this work may reflect differences in the heats and entropies of adsorption of perchlorate and/or chloride at various crystallographic planes of this metal. While the tendency of chloride to become adsorbed on metal electrodes is well-established, the same tendency for perchlorate adsorption has not yet been confirmed. However, a logical consistency of our considerations calls for an assumption that perchlorate is involved in a contact adsorption on rhodium. This inference must be checked by conducting quantitative in situ surface measurements, which are planned in our laboratory.

Since perchlorate is a very popular electrolyte in studies of the solid/liquid interfaces, we believe that the results on perchlorate reduction are of interest to many electrochemists and surface scientists who study electrode adsorption in perchlorate media.

III.2.4. Adsorption of bisulfate on cadmium, copper and silver deposits

Understanding of multicomponent electrosorption may lead to the development of **more potent electrocatalytic materials** that may offer efficient electrode activity. Electrochemical formation of ultra-thin metallic films on conducting substrates -- that enhances an additional metal/anion interaction -- clearly belongs to the multicomponent adsorption category. The thin metal deposits of monolayer dimensions are conveniently produced in the underpotential deposition (UPD) range. (The UPD electrode potential range is always more positive than the onset of the bulk deposit formation.) A remarkable progress has been made in characterization of such deposits formed on single crystal electrodes [44]. In particular, correlations have been found between the substrate surface morphology and the structural characteristics of the deposits. The research reported below was undertaken in response to the need for better understanding of metal deposition processes on the well-defined electrodes and to elucidate the nature of anion interactions with the deposits.

We have studied underpotential deposition of **cadmium, copper and silver** on gold and platinum single crystal and polycrystalline substrates [10,17,20,21,24,27,38,].

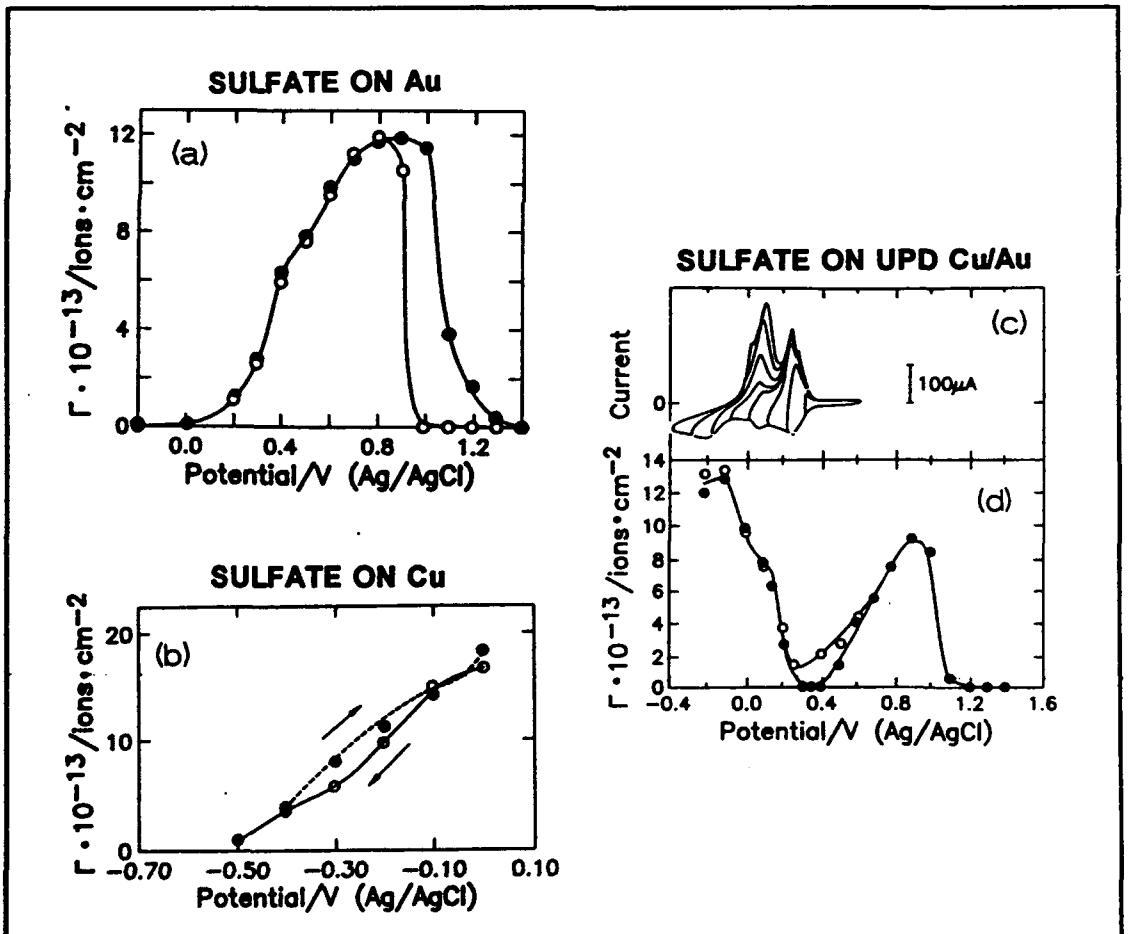

Figure 13. Demonstration of enhanced adsorption of bisulfate on the copper covered polycrystalline gold electrode (see text).

The main experimental results were adsorption isotherms, namely, anion surface concentration dependence of the electrode potential, and the companion voltammograms. In the case of silver deposition on the Au(111) electrode we have used the spectroscopies of the ultra-high vacuum science to develop a molecular-level insight into the deposition and anion adsorption processes [38].

A good demonstration of the anion adsorption on metal adatoms is bisulfate adsorption on copper adlayer on a gold surface in 0.1 M $HClO_4$ [17,24]. The copper adlayers have been obtained through electrodeposition, beginning with the underpotential deposition, Figure 13. Since no anion adsorption takes place on clean gold below 0.30 V, Figure 13a, the adsorption at potentials more negative that this value, Figure 13d, is associated with the copper electrodeposition on the gold deposit (enhanced adsorption). The threshold of the enhanced adsorption coincides with the beginning of the UPD current, Figure 13c. The second shallow adsorption maximum in the range from --0.10 to 0.20 V correlates well with the end of the copper underpotential deposition. This maximum is followed by a steady increase in the radiochemical surface count rate as the bulk deposition proceeds. Since adding copper to gold beyond the UPD region produces a copperized electrode of the thickness of a few monolayers, such a newly created surface will tend to adsorb anions in a manner similar to the clean copper, Figure 13b.

The surface concentration obtained as a function of the electrode potential for bisulfate adsorption on the clean Au(111) electrode, and on the Au(111) electrode covered by silver, are shown in Figure 14 (see Figures 4c and 5c for the

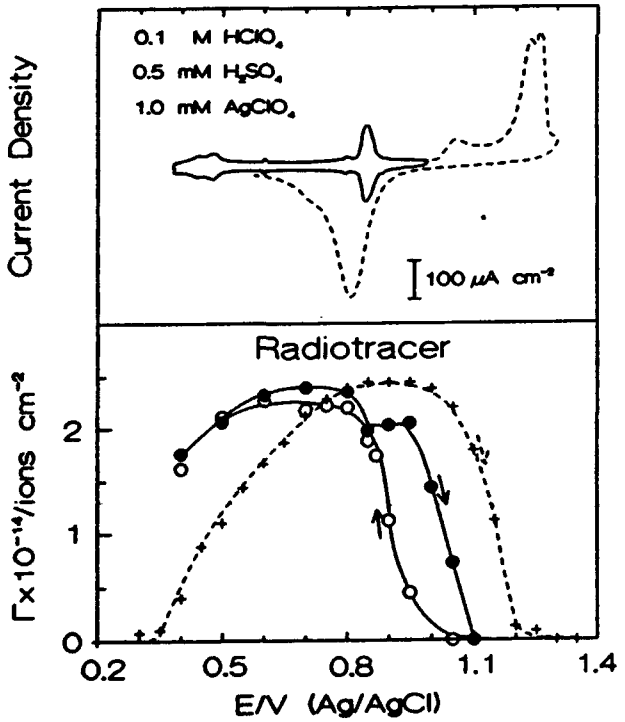

Figure 14. Radiochemical measurements of enhanced adsorption of bisulfate on the silver covered Au(111) electrode. Comparison with the companion voltammetry. (+) adsorption of bisulfate on the clean Au(111) electrode.

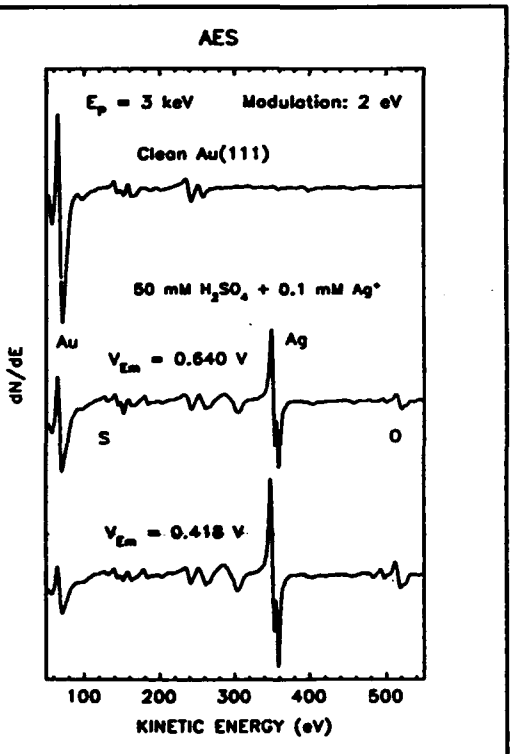

Figure 15. Auger electron spectra of clean and silver covered Au(111) electrode. The electrode potentials of the UPD process is indicated as V_{Em}. Beam energy (E_p) = 3 keV.

radiochemical and voltammetric characterization of the clean Pt(111) surface [38]). There is a very good correlation of the Γ vs. E plot and the details of the current-potential voltammetric curve that accounts for the deposition/stripping processes. Auger electron spectroscopy measurements, Figure 15, give data consistent with those produced by radiochemistry [38]. We have also measured LEED patterns of the Au(111)/Ag system obtained in sulfuric acid solution through the underpotential electrodeposition process. The pattern corresponds to a Au(111)(5 x 5) surface structure, Figure 16. This is a very interesting observation since silver deposition on a "dry" surface of gold has given a (1x1), pseudomorphic surface configuration [45]. Moreover, previous in situ imaging work by AFM and STM of silver UPD process gave the Au(111)(3x3)-Ag structural arrangement [46,47]. We are prompt to add that our data have been obtained after extensive electrode rinsing before the transfer to the UHV. This left approximately 0.1 ML of bisulfate on the electrode surface in the UHV. In contrary, the in situ surface concentration of the bisulfate on the silver deposit on (111) gold is most probably closer to 0.3 ML. The next experimental step is to decrease the number of rinsing and see if the (3x3) structure is found in the process.

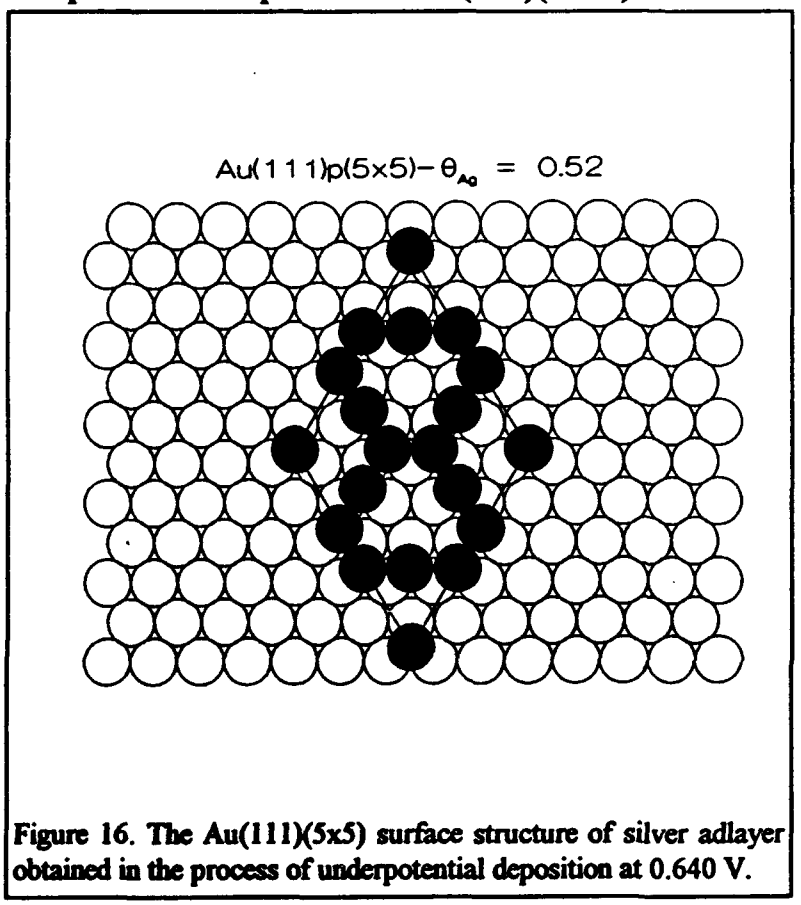

Figure 16. The Au(111)(5x5) surface structure of silver adlayer obtained in the process of underpotential deposition at 0.640 V.

A potential dependence of ^{35}S-labeled bisulfate adsorption on the ordered Pt(111) electrodes in the presence of 10^{-3} M Cd^{2+}, Cu^{2+} and Ag^{+} in solution, and the companion voltammograms, are shown in Figures 17, 18 and 19, respectively. The solution composition was 0.1 M $HClO_4$ + 10^{-3} M of the cations and 10^{-4} M of H_2SO_4. A careful analysis reveals some interesting details of the correlation of the enhanced bisulfate adsorption and the charges corresponding to the deposition process. In the case of cadmium [20,24], a clear adsorption of bisulfate on the admetal-covered Pt(111) electrodes begins at 0.2 V and continues down to -0.15 V, Figure 17-a, segment 2. At 0.20 V, as shown in Figure 17-b, the cadmium deposition process is already advanced (in fact, complete in nearly 30% [20]). That is, the enhanced bisulfate adsorption is not caused by the formation of the UPD cadmium phase deposited in the utmost positive potential range. This is contrary to what we have observed with gold (see above and ref. 17). This initial observation of the non bonding properties of the cadmium deposits with

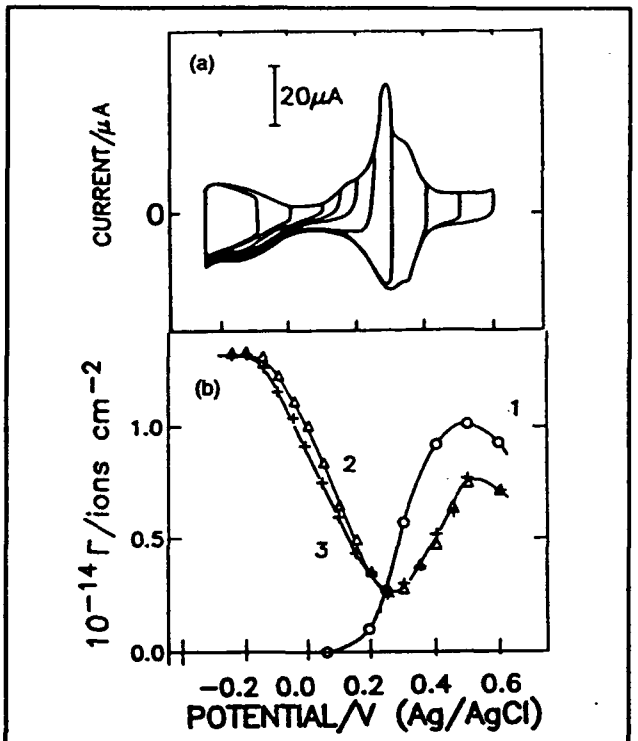

Figure 17. (a) - a voltammogram and (b) - potential dependence for Cd-UPD on Pt(111) in 0.1 M $HClO_4$ + $3x10^{-4}$ M Cd^{2+} + 10^{-4} M H_2SO_4 at 10 mV·s^{-1}: curves 2 and 3. Curve 1: 0.1 M $HClO_4$ + 10^{-4} M H_2SO_4.

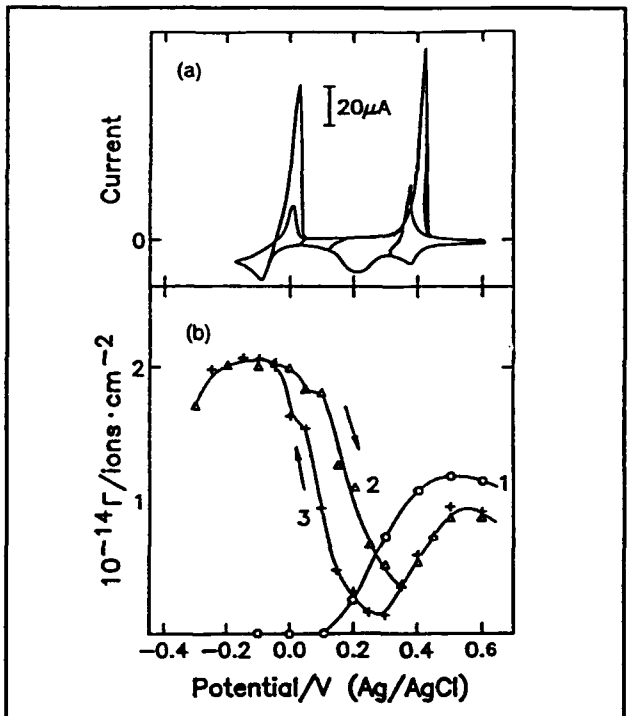

Figure 18.(a) - a voltammogram and (b) - potential dependence for Cu-UPD on Pt(111) in 0.1 M $HClO_4$ + $3x10^{-4}$M Cu^{2+} + 10^{-4} M H_2SO_4 at 10 mV·s^{-1}: curve 2 and 3. Curve 1: in 0.1 M $HClO_4$ + 10^{-4} M H_2SO_4.

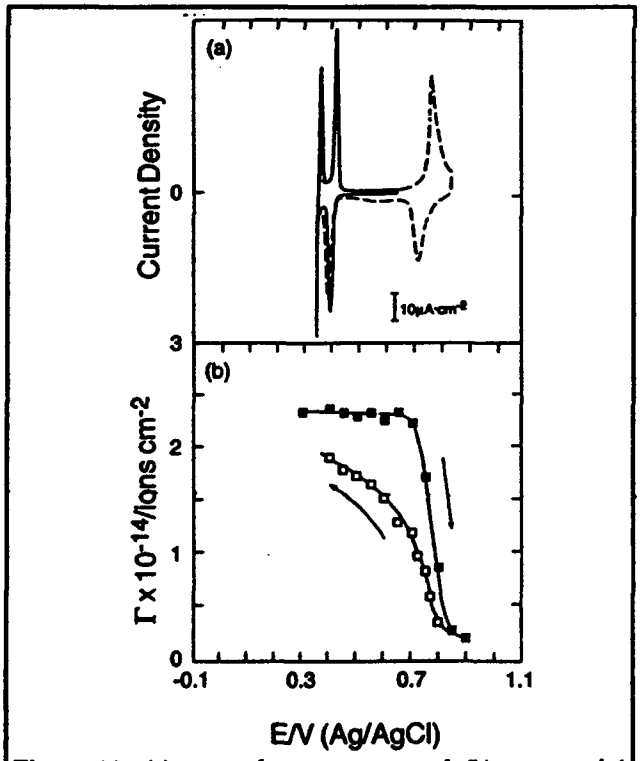

Figure 19. (a) - a voltammogram and (b) - potential dependence for Ag-UPD on Pt(111) in 0.1 M $HClO_4$ + 10^{-3}M Ag^+ + 10^{-4} M H_2SO_4 at 10 mV·s^{-1}.

respect to solution bisulfate has been reaffirmed during the studies of copper deposition on platinum, Figure 18; an increase in bisulfate adsorption begins at the electrode potential not lower than 0.30 V. One should also notice that bisulfate desorbs from the Cu-coated surfaces before the stripping of copper from platinum begins. Since no faradaic processes is coincident with the desorption process, we believe we have a clear evidence that the surface bisulfate anion is substituted by perchlorate.

If two electrons are transferred upon the UPD deposition, the electric charge gives electrochemical estimate of the copper coverage on the electrode surface. The UPD charge obtained at a slow scan rate (5 mV·s^{-1}) is large enough to account for formation of more than 90% of copper monolayer, showing that nearly a closed-packed monolayer of the neutral

copper adatoms may be formed on platinum. However, recent spectroscopic data indicate [48] that the valency of the underpotentially deposited copper is +1, and that some electron charge is donated to platinum through partial filling of the empty d-bands vacancies. We may tentatively propose the following formal reaction scheme to satisfy both spectroscopy and coulometry:

$$Pt + Cu^{2+} + 2e^- = (Pt^-)\text{-}Cu^+ \qquad (1)$$

with the second electron remaining on the platinum side of the interface. If this reaction scheme is correct, the Cu^+ surface species represents the site for bisulfate adsorption. Both perchlorate and bisulfate may compete for such a species with bisulfate becoming progressively more strongly adsorbed than perchlorate when potential is more negative than 0.35 V.

We conclude that the results expose an issue that has not yet been strongly emphasized in the earlier literature on ultra-thin metal electrodeposits. Namely, we have observed a formation of not only anion-active, but also inactive UPD films. In the case of cadmium UPD, the reasons for the inactivity is cadmium oxidation. With the copper deposit, the perchlorate anion -- that is present in 10^3 excess to bisulfate -- replaces the surface bisulfate adsorbed at more negative potentials. To our knowledge, the formation of such inactive metal adatoms has not been anticipated with the metals studied in this project.

The information on adsorption of bisulfate on silver adlayers on the Pt(111) electrode is presented in Figure 19 [27]. The enhanced adsorption is mainly observed in the potential range where silver should be stripped from the Pt(111) surface by the positive going potential excursion. Evidently, some form of silver remains on the electrode at the most positive potentials used in this study. Since this is a relatively high electrode potential range, UPD silver (and some platinum surface atoms) are probably in the oxide form [27]. A hysteresis in bisulfate adsorption decreases with the increase in the bulk concentration of sulfuric acid in the perchloric acid electrolyte, suggesting that adsorbed bisulfate anions approach the saturation level at 10^{-3} M. These are new observations that require an advanced theoretical treatment.

We also notice that the main voltammetric features associated with these UPD silver phases are extremely well-resolved. Likewise, a third phase, not yet reported for the clean Pt(111) electrode, and that yields a deposition voltammetric transition in the potential range of 0.65 to 0.45 V, is seen. Apparently, with enough care in the crystal preparation, the voltammetric features follow the behavior of silver on the iodine coated Pt(111) surfaces [49]. Perhaps surprisingly, and in contrast to the quoted Pt(111)-I-Ag work, silver electrodeposition in the intermediate potential range is virtually irreversible. It should also be added that only a small modification of the voltammetry is made when 0.1 mM of sulfuric acid is added to the cell.

III.2.5 UPD silver and iodine coadsorption on the Rh(111) electrode

Using the UHV methodology and the Rh(111) electrode covered by iodine, we have obtained data that are relevant to the deposition processes referred to above and in ref. 49. The starting substrate was that denoted as Rh(111)($\sqrt{3}$x$\sqrt{3}$)-Θ_I = 0.35 [4]. The deposition of silver gives rise to the voltammetry shown in Figure 20 (the symbols A_S denote silver adsorption (deposition) processes and the D_S: silver dissolution). The main events are those indicated as A_4/D_4 and A_5/D_5. In the saddle point between the two deposition pairs, A_4 and A_5, where approximately a monolayer of silver was deposited, a weak but clear LEED pattern was found after emersion to the UHV, Figure 21. Both integral and the fractional spots are split (the "$\sqrt{3}$" spots being most probably due to the ($\sqrt{3}$x$\sqrt{3}$) structure of the chemisorbed iodine) indicating a multi-domain surface arrangement of the adsorbates, ref. 4 and references quoted therein. *The AES data have given evidence for an intercalation of silver monolayer electrodeposits between the adsorbed iodine plane and the substrate surface. This shows that the intercalation mechanism is not limited to platinum.* The details of the silver transfer underneath the iodine adlayer are still not clearly understood, despite the fact that an advanced treatment has recently been devoted to this subject [50].

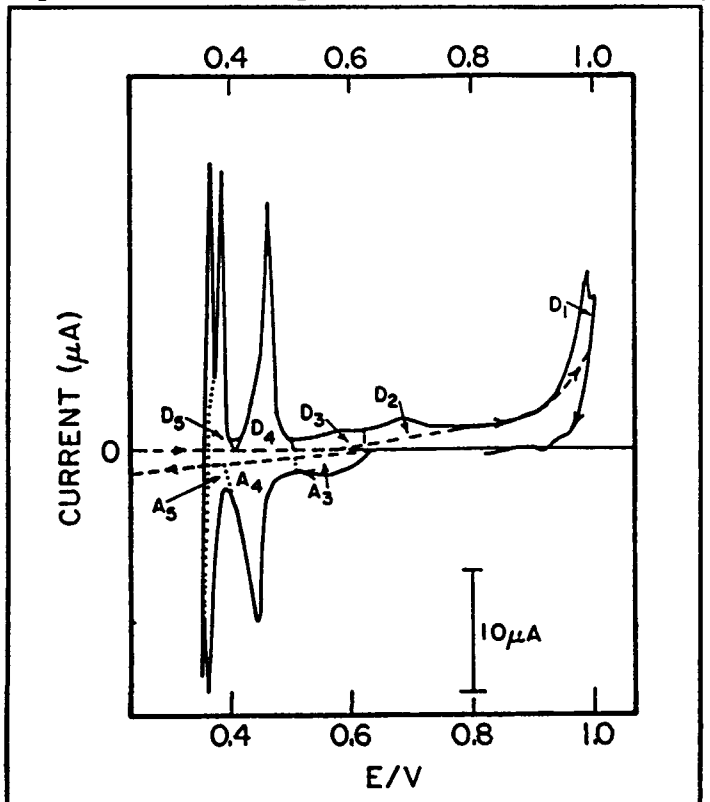

Figure 20. The underpotential deposition of silver on an iodine-coated Rh(111) electrode at 2 mV·s^{-1} in 1.0 M $HClO_4$ + 10^{-3} M Ag^+. (—) date in 1.0 M $HClO_4$ (see text).

III.2.6. Palladium deposits on the Pt(111) substrate in vacuum

We have also investigated monolayer palladium deposits on the Pt(111) surface formed in ultra-high vacuum using the XPS, AES and LEED techniques [31]. This work was dedicated to account for the unique voltammetric behavior of single crystal platinum electrodes covered by palladium monolayers in the hydrogen range of the electrode potentials (ref. 50 and references quoted therein). In particular, the origin of the two narrow voltammetric peaks with the Pt(111) electrode at 0.22 V and 0.45 V (vs. RHE) is not yet well-understood. We began this research in attempt to explain the voltammetric observations on the molecular and quantitative level, and compare the UPD of palladium with the "dry" palladium deposition on the Pt(111) surface. The data on the dry Pd/Pt(111) interface, required for the comparison, have not been available in the

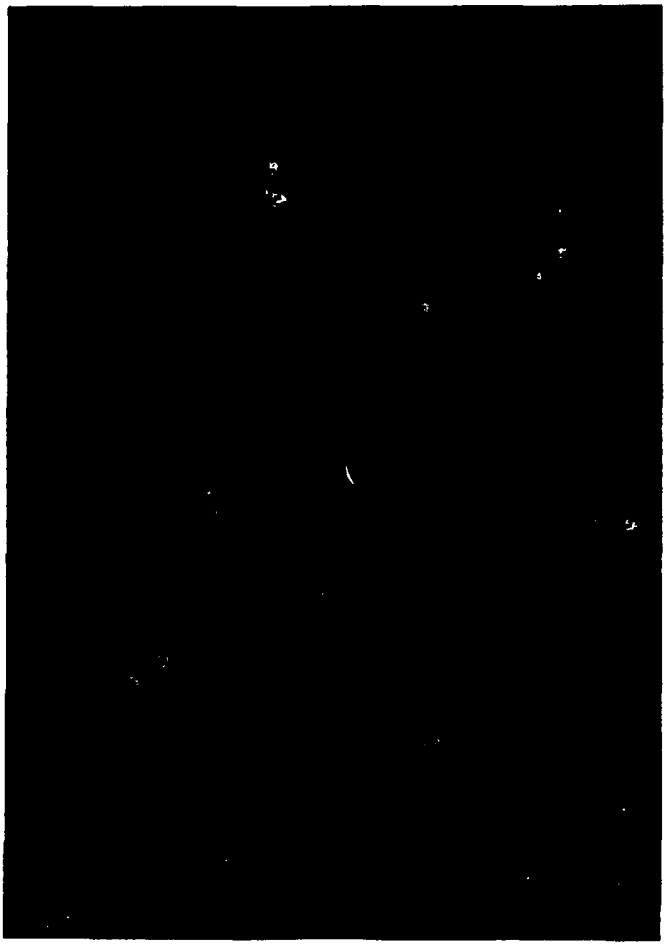

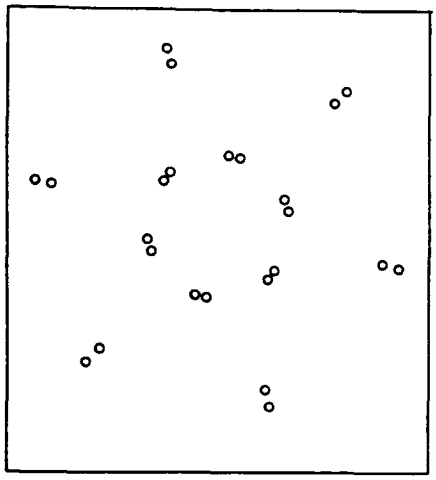

Figure 21. The LEED pattern and diagram for the Rh(111)-I electrode containing 1 ML of UPD silver. See Figure 20 and text. The beam energy was 46.2 eV.

surface science literature, other work is referenced in our ref. 31.

In this report, we will focus on the electronic configurations by XPS, and their possible connections with voltammetry. The voltammetric and electrodeposition measurements have also been conducted and will be presented elsewhere.

The raw and deconvoluted X-ray photoemission spectra corresponding to the core levels of Pd 3*d* and Pt 4*d* are shown in Figure 22. The deconvolution was made using a non-linear, least-square-fit method. The results give a Pd $3d_{5/2}$ core-level binding energy of a 334.9 eV at coverages below 0.4 ML. Usually, the electron core-level binding-energy in metallic clusters increases upon decreasing the coordination number due to a poorly screened final-state effect. Therefore, one could anticipate that during deposition the palladium core-level binding energy should be the highest at low coverages, and be followed by a binding-energy decrease with the increase in palladium coverage. Unexpectedly, the results of our study show an opposite trend: the higher the palladium coverage, the higher the Pd 3*d* binding energy, Figure 22c: the binding energy increases by 0.2 eV and flattens when about two monolayers of palladium are obtained. At 4.0 ML coverage, the binding energy is 335.3 eV.

This positive BE shift from low coverages toward the bulk value has already been predicted by Wertheim and Citrin [51], but not experimentally confirmed at that time. The quoted authors have concluded that the 4*d* valence- and 5*s* conduction-bands of Pd

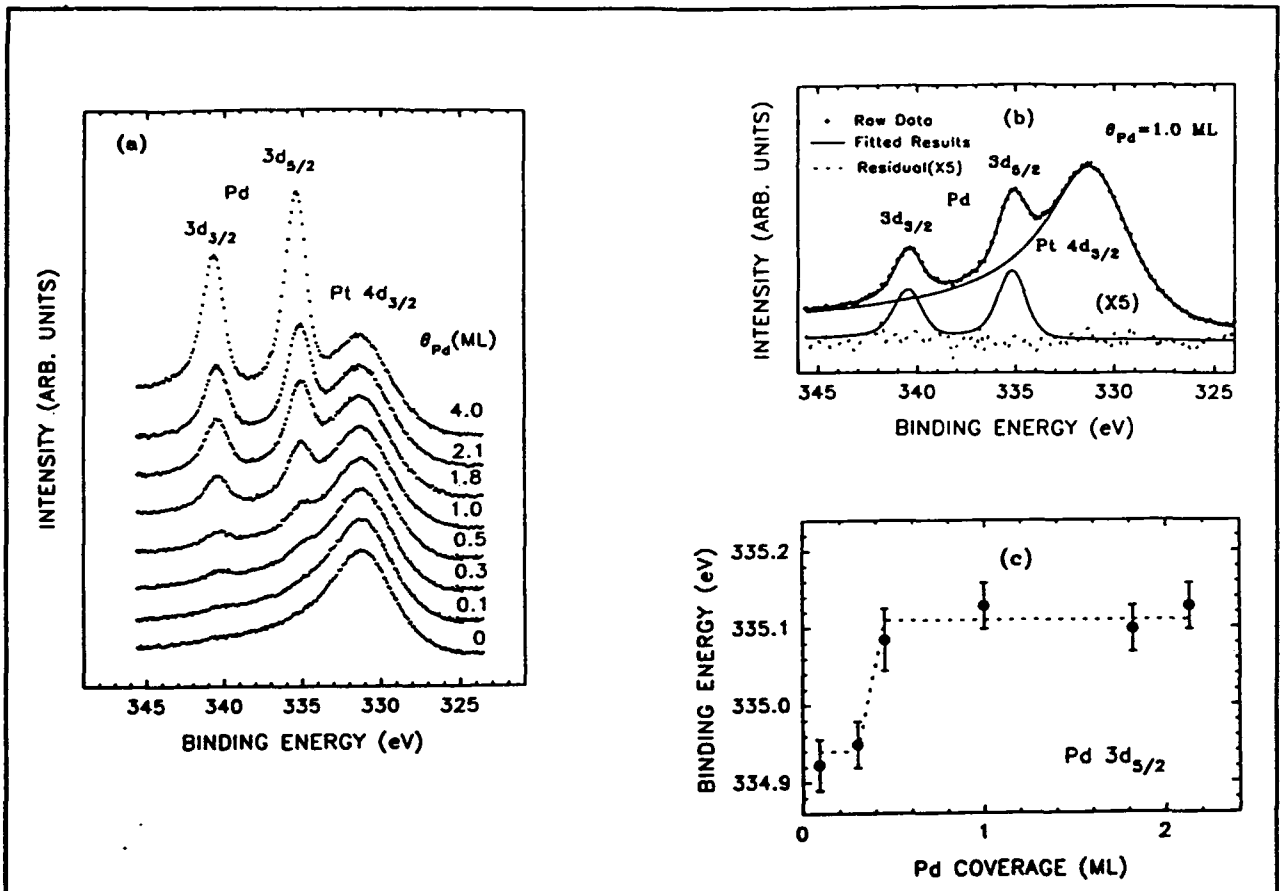

Figure 22. XPS results of Pd adlayers deposited in UHV on Pt(111): (a) Pd 3*d* and Pt $4d_{3/2}$ core-level spectra, (b) the same as in (a) but at Θ_{Pd}=1.0 ML and the fitted results. (c) - binding-energy shift of Pd the $3d_{5/2}$ core-level as the Pd coverage varies.

should narrow and separate from each other with decreasing size of palladium clusters. As a net result, the intra-atomic charge transfer should occur, thus moving the system toward the $4d^{10}$ configuration of the free Pd atom. To preserve the charge neutrality, each atom keeps the same number of occupied electronic states. Therefore, the centroid of the valence-band [31], as well as the surface-atom core-levels, move towards vacuum level.

The absence of the final-state effect after creating a core-hole in the Pd/Pt(111) system indicates that an efficient hybridization of the valence bands of the palladium adlayer and the platinum substrate has an important role in the surface atom binding-energy shift of the Pd 3*d* core-level. If an equivalent Pd/Pt(111) interface is created via electrodeposition, we may tentatively assume that the first chemical interaction of the solution proton is with the hybridized surface valence bands. This is accompanied by an electron charge transfer from the metal electronic energy level to proton. Since hydrogen dissolves well in palladium, the H atoms may easily penetrate the first palladium monolayer to become intercalated between this first layer and the Pt(111) substrate. This preliminary explanation of the voltammetry needs to be expanded to obtain further theoretical insight.

Summarizing the main findings reported in the chapters III.2.4-6 of this proposal, we may conclude that the most probable reasons for the lack of activity of cadmium covered platinum toward bisulfate is that a cadmium oxide(s), instead of cadmium adatoms, are deposited at sufficiently positive potentials. With some exceptions, oxidized metal surfaces do not adsorb anions. With the copper UPD covered platinum electrodes, the surface-chemical forces that bind bisulfate, with respect to those between the metal and perchlorate, are dominant when the electric field weakens with the positive going electrode polarization. (Notice that perchlorate was the majority anion in the measurements.) Since such a replacement process has not been observed with the Au/Cu substrate, we conclude that the Pt/Cu electrode has stronger affinity to perchlorate than the Au/Cu electrode. This demonstrates a significance of the nature of the support in chemical properties of the metal deposits of monolayer dimensions. Similar conclusions have been made with silver covered platinum and gold.

The data obtained with palladium deposits on the platinum (111) substrate and silver adlayers on the Rh(111) electrode, although already published, are considered preliminary. They lay foundation for new research that will be pursued in this laboratory. Notably, we have observed an intercalation of some adsorbed or deposited species on some multicomponent surfaces: silver underneath a bisulfate adlattice [27], silver in between iodine adlayer and the Rh(111) surface (see ref. 49 for Pt) and hydrogen between palladium UPD monolayer and the platinum (111) surface. Stuve is also reporting hydrogen intercalation in the graphitic carbon/platinum (111) surface [52]. We conclude that an intercalation process may occur in surface electrochemistry more often than it has been believed.

III.3. Adsorption of carbon monoxide on catalytic single crystal surfaces

The focus on surface chemistry of **carbon monoxide in electrochemistry** arises predominantly from its adverse poisoning role in methanol fuel cell applications [4,8,23,25,30]. Through our planned and recently executed work on methanol electrocatalysis, reported in section III.1 of this proposal, we have become interested in the poisoning phenomena. We have focused on surface electrochemistry of carbon monoxide since the earlier and current data designate surface CO as the methanol main chemisorption product. The CO chemisorbate is most likely composed of a mixed population of the carbon monoxide molecules that coordinate the surface via linear and bridge bonded configurations. We have investigated the CO adsorption on the Pt(111), Pt(100) and Rh(111) electrodes in the CO saturated perchloric and sulfuric acid solutions by a combination of the low energy electron diffraction, Auger electron spectroscopy and electrochemistry.

The electrode potential for carbon monoxide adsorption on the Pt electrodes was -0.20 V. Higher potentials were avoided in order to reduce the possibility of surface CO oxidation during system evacuation. The CO chemisorption on rhodium is stronger and was easily studied by the UHV technique also in the double layer of the electrode potentials (0.15 V). After completing the adsorption phase of the experiment the electrode was rinsed repeatedly with electrolyte that did not contain CO to remove the traces of the unbound CO solute. The adsorbate was either oxidized in a positive-going

voltammetric scan, or transferred to the UHV chamber for the LEED and AES characterization.

The results concern the structure, reactivity and surface coordination of the CO adsorbed on the three chosen single crystal surfaces. The main data are summarized in Figures 23-27. The LEED data at saturation coverage (roughly 0.8 ML), shown in Figure 23a, c and d on the Pt(111), Pt(100) and Rh(111) electrodes give the ($\sqrt{3}$ x 3)rect.,

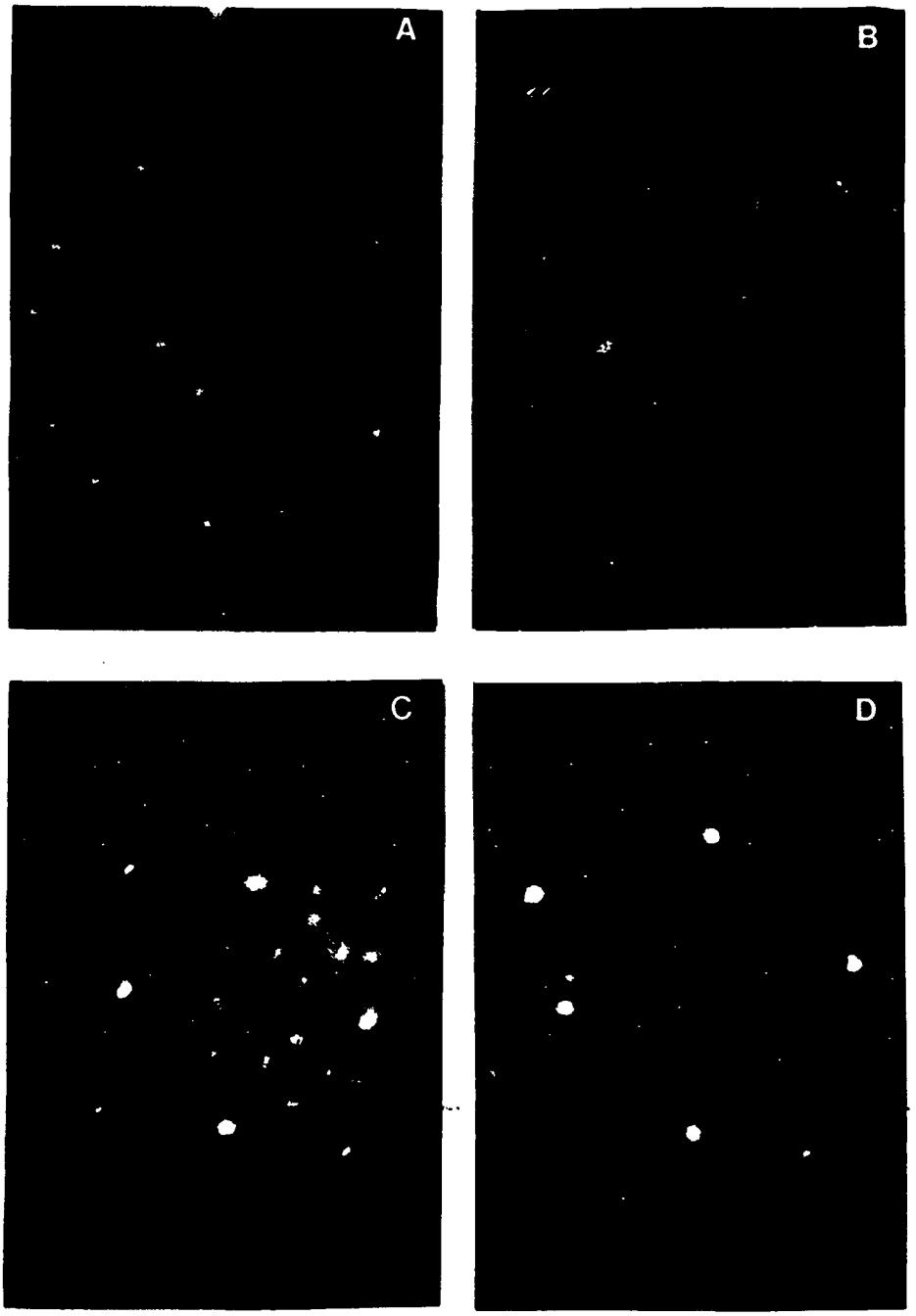

Figure 23. LEED patterns for the Pt(111)($\sqrt{3}$ x 3)rect, Pt(111)c($\sqrt{3}$x5)rect, Pt(100)c(4 x 2) and Rh(111)split(2x2) surface structures of electrosorbed CO. Beam energy in the range of 40-60 eV.

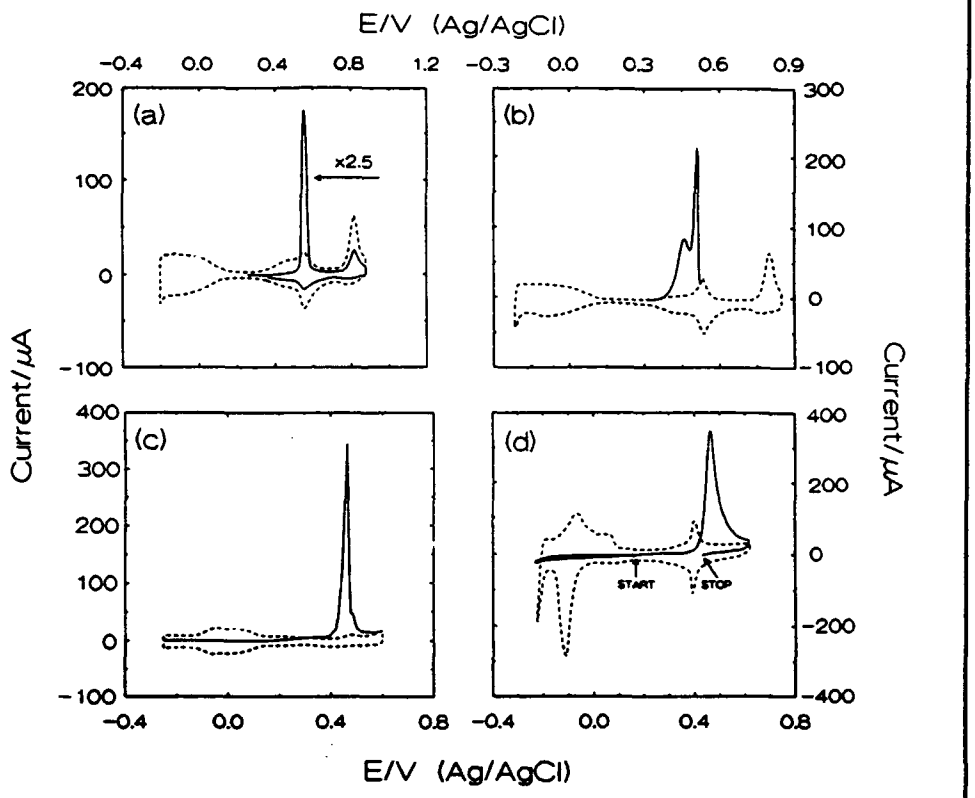

Figure 24. Voltammograms corresponding to the surface structures of electrosorbed CO in Figure 23 in perchloric acid electrolyte (50 $mV \cdot s^{-1}$). The baselines in the clean supporting electrolyte are shown by the dashed profiles.

c(4x2) and split(2x2) surface structures, Figures 25a, c and Figure 26, respectively (the companion voltammograms are shown in Figure 24). These are the same structures as in the earlier gas phase studies of the equivalent surface systems. The corresponding data for the CO coverage of ca. 0.6 ML (LEED pattern, voltammetry and the Pt(111)c(√3x5)rect structure, Figure 23b, 24b and 25b, respectively) are also in agreement with the gas phase results. At even lower coverage, we have found islands possessing internal organization of these high-packing structures. However, the stability of such islands is limited and a slow structural rearrangement of the Pt(111)(√3 x 3)rect, or Pt(111)c(√3x5)rect, to a Pt(111)c(4 x 2) surface structure occurs.

Control of emersion process

The emersion control experiment is demonstrated below for the Pt(100) electrode [30]. The CO covered electrodes were transferred to the UHV for a period of approximately 20 minutes, and transferred back to the electrochemical cell for the voltammetric characterization. Table 2 (second row) contains charges needed for the oxidation of the chemisorbed CO, and the derived CO coverages obtained after correcting for the double layer charge [30]. In sulfuric acid solution, the mean CO coverage was 0.75 ± 0.07, Table 2. This is the same coverage (within the experimental error) as that obtained before the UHV exposure. In perchloric acid, the post evacuation coverage was lower than the value obtained before the UHV exposure. However, the c(4x2) LEED

Table 2. The total CO stripping charge (q^{CO}), the stripping charge after the double layer correction (Q^{CO},), and the CO coverage (Θ^{CO}) obtained from Q^{CO}. Carbon monoxide was dosed at -0.200 V in electrolytes specified in the first column of the Table.

	q^{CO} ($\mu C/cm^2$)	Q^{CO} ($\mu C/cm^2$)	Θ^{CO} (ML)
0.5 M H_2SO_4	488±20	322±20	0.77±0.04
0.5 M H_2SO_4 after UHV	470±30	314±30	0.75±0.07
0.1 M $HClO_4$	500±30	335±30	0.79±0.07

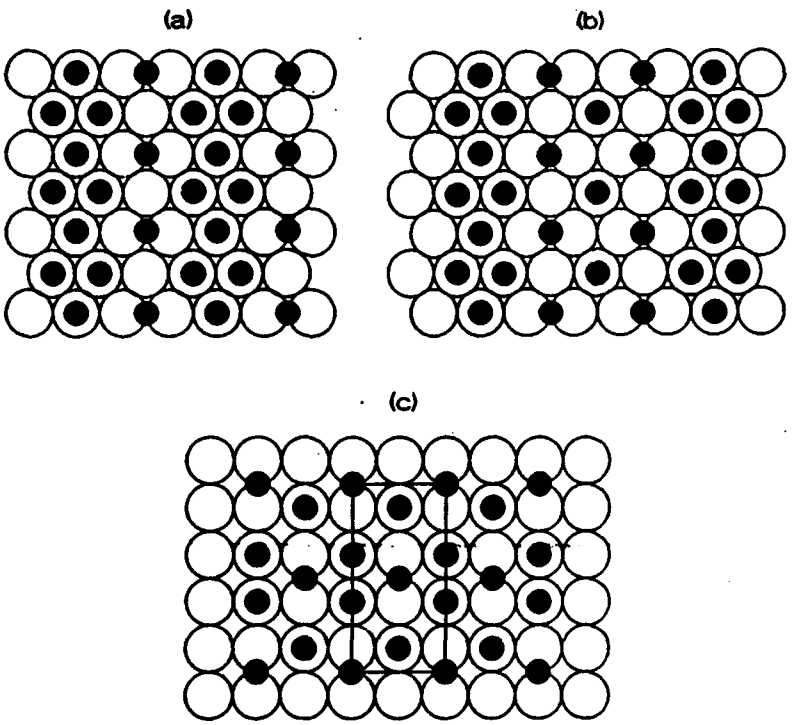

Figure 25. The surface structures corresponding to the LEED patterns in Figure 23a-c.

pattern, Figure 23c, was consistently observed with a varying amount of the background intensity. We conclude that some desorption of CO was taking place. The desorption most likely occurred via oxidation of surface CO by perchlorate vapor during the Pt-CO sample re-immersion. Therefore, the electrolyte that guarantees a successful, desorption free outcome of the electrochemistry-vacuum transfer

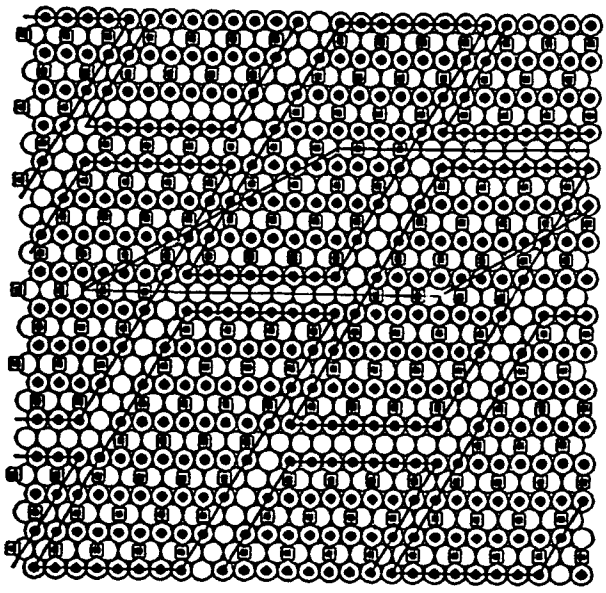

Figure 26. The surface structure corresponding to the LEED pattern in Figure 23d.

experiment with the CO adsorbate is a dilute sulfuric acid rather than perchloric acid.

The details concerning carbon monoxide adsorption on the Pt(111) and Rh(111) electrodes have already been published [4,8,23,25,] and reported for AFOSR [1]. Not yet reported, but accepted for publication data [30], were obtained with the Pt(100) electrode. This includes a detailed spectroscopic study by AES and the structural analysis by LEED, Figure 23c and Figure 25c. The secondary electron spectrum of the clean Pt(100) surface, taken at a primary electron beam energy of 800 eV, is shown in Figure 27. The major Pt Auger electron transitions are: 64 eV, 150 eV, 168 eV, 237 eV, 251 eV. The interesting features of this spectrum are the loss peaks appearing at kinetic energies 480 eV 462 eV and 449 eV. The first two peaks are due to the $N_5(4d_{5/2})$ and $N_4(4d_{3/2})$ electrons of platinum excited into empty states above the Fermi level. These spectral features correspond to the energy losses of around 316 eV and 333 eV below the primary electron energy, in agreement with the literature data. The third loss peak, 30 eV below the N_5 ionization peak, is due to a single plasmon loss (the free electron Pt plasmon energy is 30.2 eV). The information on the Auger electron transitions of carbon monoxide adsorbed on the Pt(100) surface in gas

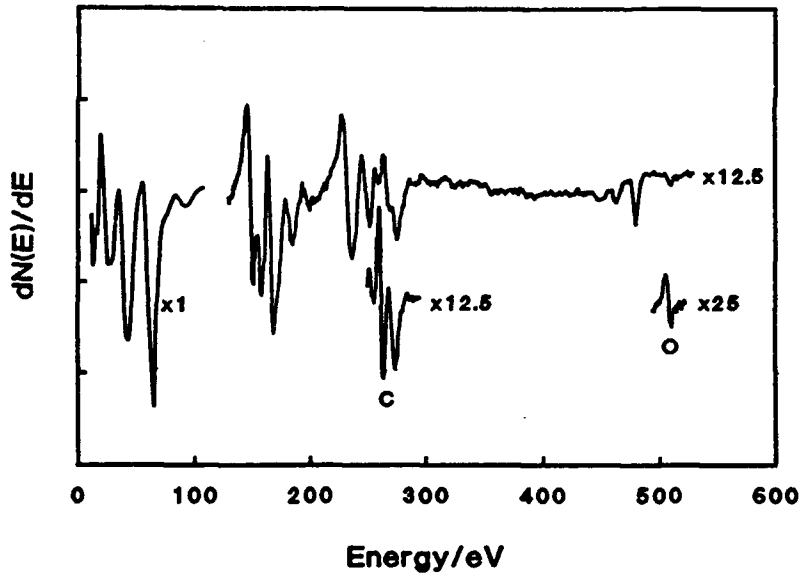

Figure 27. Auger electron spectrum of the Pt(100) crystal covered by electrosorbed CO in 0.1 M H_2SO_4 solution. Bean energy 800 eV.

phase is not yet available. The present analysis, aimed at assigning the spectral features observed in this study to the previously published ones, is made using AES data on CO adsorption on other than Pt(100) metal substrates, and on an organometallic compound ($Mo(CO)_6$, Table 3). The analysis shows that the relative AES peak energies fall into three different classes. The transition marked as peak 1 is around 10 eV above peak 3, the transition represented by peak 2 appears close to 7 eV above peak 3, while the AES transition denoted as peak 4 is around 8 eV below peak 3. The transition observed presently at 272.9 eV is 10.3 eV above peak 3. This suggests the ($5\sigma/1\pi,2\pi$-d) final two hole configuration as for the CO/Pt(111) surface system. The most recent results for the

Table 2. Carbon Auger energies in carbon monoxide on metal surfaces and in $Mo(CO)_6$.

Substrate	Peak no.			
	1	2	3	4
$Mo(CO)_6$ gas	264.0	261.0	255.0	249.0
energy dif.	-9.0	-6.0	0.0	6.0
CO/Cu(111)	279.5	275.5	270.0	261.0
Energy dif.	-9.5	-5.5	0.0	9.0
CO/Cu(100)	276.7	273.6	267.3	258.0
Energy dif.	-9.7	-6.4	0.0	9.3
CO/Ni(111)	-	274.4	267.3	260.2
Energy dif.		-7.1	0.0	6.9
CO/Ni(100)	-	275.7	269.0	260.0
Energy dif.		-6.7	0.0	9.0
CO/Pt(poly)	-	272.0	264.0	-
Energy dif.		-8.0	0.0	
CO/Pt(111)	279.5	275.5	268.5	259.5
Energy dif.	-11.0	-7.0	0.0	9.0
CO/Pt(111)	280.0	-	270.0	260.0
Energy dif.	-10.0		0.0	10.0
CO/Pt(111)	275.6	273.1	264.6	257.5
Energy dif.	-11.0	-8.5	0.0	7.1
CO/Pt(100)	272.9	-	262.6	254.3
Energy dif.	-10.3		0.0	8.3

latter system show four, instead of three, distinct peaks, but peak 2 has the lowest intensity [53]. The relative positions of peaks 1, 3, 4 in the spectra presented here are in accord with the platinum/CO data of ref. 52. Peak 2 is not found in Figure 1b presumably because of its low intensity. The assignment of peaks 3, 4 in CO/Pt(100) is not definite, but the real situation cannot be much different from that for CO/Ni(100) describing 3 as $(5\sigma,5\sigma)$, $(5\sigma,1\pi)$, $(1\pi,1\pi)$ and 4 as $(4\sigma,4\sigma)$ final two hole configuration [54]. Peaks 3, 4 are, most likely, of the intramolecular origin. *On the basis of the above analysis, we conclude that there is a clear similarity in the spectral appearance of the chemisorbed CO from the gas phase and that obtained under electrochemical conditions.*

According to Biberian and Van Hove [55], the general notation of Pt(100)c(2x4)-Θ_{CO} = 0.75 may embody four ifferent structures that differ as to the intimate details of surface coordination by the bridge- and terminal- bonded CO molecules. From these four structures we chose the one shown in Figure 25c as most closely corresponding to our electrochemistry data. (Using earlier vibrational measurements [56,57] we knew that the population of the terminal CO is predominant over the bridge-bonded population, like in Figure 25c. Also, for the (100) platinum substrates characteristic of the long range surface order, the bridge-bonded CO is adsorbed in a symmetric configuration.) In this structure, there are 33% of the CO molecules in the symmetric bridge-bonded configuration, and 67% of the CO molecules in the terminal coordination, with the 0.5 ratio of the bridging/terminal CO populations. We believe we have evidence that the surface configuration of CO adsorbed at the threshold of hydrogen evolution is the same as that observed after the gas phase adsorption to the Pt(100) substrate. As shown above, the unit cell for this configuration is Pt(100)c(4x2)-Θ_{CO} = 0.75, and the experimentally measured CO coverage is 0.77 ± 0.04 molecules per platinum surface site.

We conclude that the adsorbate obtained on the three single crystal surfaces studied in the CO saturated solutions, and emersed to the UHV for surface analysis, has the necessary characteristics of surface CO already observed in gas phase. Specifically with the Pt(100) electrode, the population ratio of the bridge-bonded and terminal bonded CO obtained in solution is in the category of the ideal 0.33 : 0.67 ratio in the Biberian diagram [55]. The solid/liquid surface CO is stable, or can be made stable, during the solution-UHV-solution transfer. In a broader perspective, the gas phase and electrochemistry comparison practiced in this work may allow one to develop diagnostic clues on the similarities and differences between the solid/liquid and solid/gas interfaces. This, in turn, may unveil the role of solvent and the electrode potential in formation of adsorbate layers in electrochemistry.

III. 4. Phase transitions induced by lateral adsorbate-adsorbate interactions (urea)

When interacting with platinum electrodes, the behavior of some neutral molecules, specifically urea and saturated carboxylic acids, resembles that of surface active inorganic anion [58,59]. Phenomenologically, this due to a combination of some distinctive molecular features of these organic neutrals, and their high molecular bond stability on platinum. Therefore, the studies of these neutral adsorbates have been in the interests of this program. The investigations reported below have mainly focused on urea

since the voltammetry of platinum electrodes in the urea-containing solutions is more resolved than in the acetic acid containing solutions.

In collaboration with Professor P. A. Rikvold, FSU, we presented voltammetric data for adsorption of urea on the single-crystal Pt(100) electrode [15]. The most striking feature of the cyclic voltammograms for this system was the replacement of the relatively wide, symmetrically located, hydrogen adsorption and desorption peaks in the urea-free voltammogram by sharp peaks when urea was present. This voltammetric change was of a magnitude and sharpness not previously observed with neutral adsorbates in a non-oxidative electrode potential range. Recently, we have obtained the experimental data necessary for theoretical lattice-gas modeling of the electrosorption of urea on this Pt(100) electrode. These include cyclic voltammetry profiles and analyses of voltammetric peak widths and positions vs. sweep rate, adsorbate structure by the low-energy electron diffraction, and urea coverage by radioactive labeling and Auger Electron Spectroscopy [39]. Using the experimental data, we have developed a lattice-gas model for coadsorption of urea and hydrogen on this surface. The model is presented and results of the numerical Monte Carlo simulations are compared with the measurements, showing excellent agreement. This is the first time such an integrated study of the electrosorption of an organic substance has been performed.

The main experimental results are as follows. For electrode potentials on the positive side of the CV peak somewhat diffuse, but clear, c(2x4) LEED patterns are observed, Figure 28. These disappear close to the voltammetric peak and are absent on the negative side of the voltammetric transition range. Furthermore, the urea coverage, measured both by radioactive labeling and AES, Figure 29 and 30, falls from near 1/4 urea molecules per Pt(100) unit cell in the positive potential region to near zero on the negative side of the current-potential peak. The Auger electron spectrum shows that all three urea elements are present on the surface. Since

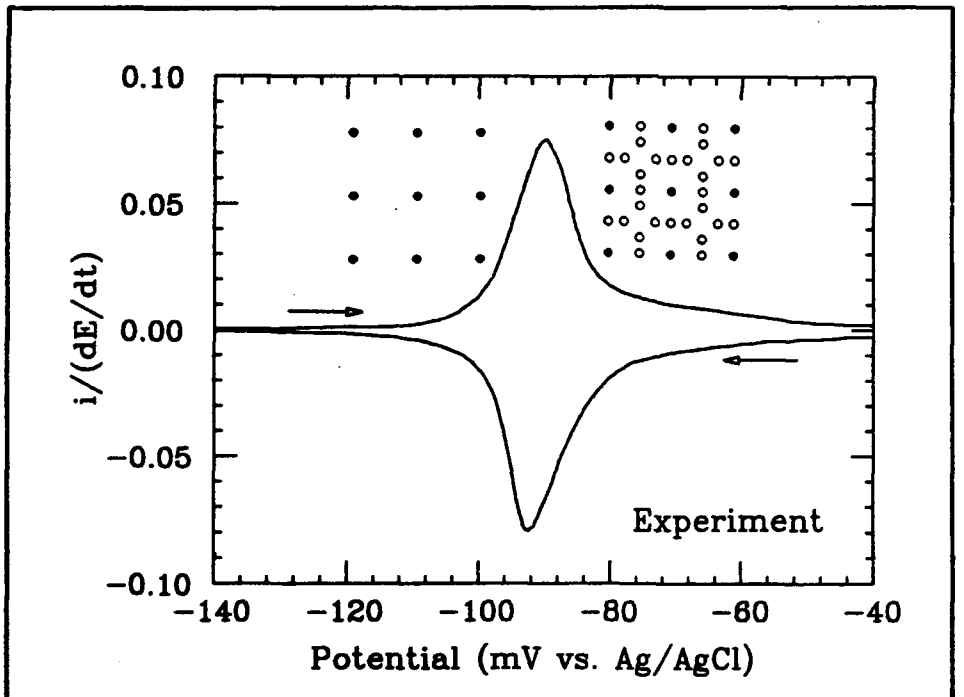

Figure 28. Cyclic voltammogram of the Pt(100) electrode in 0.1 M $HClO_4$ + $5x10^{-4}$ M urea at 50 mV s^{-1}. Also shown are LEED diagrams for the unreconstructed Pt(100) surface and the Pt(100)c(4x2)-urea surface structure (see text).

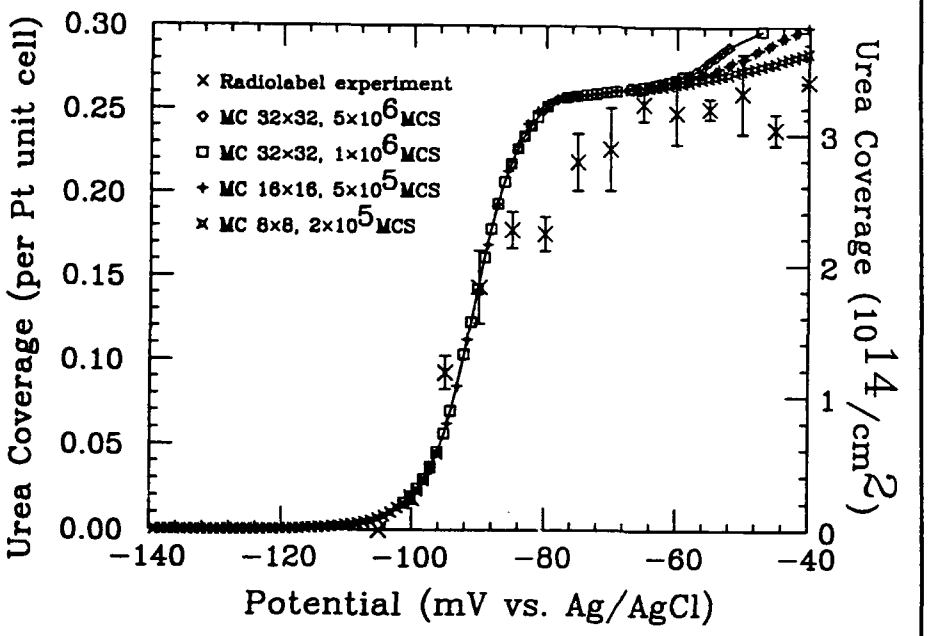

Figure 29. Experimental and simulated urea coverage vs. electrode potential results. The experimental data (x, with error bars) were obtained by a radioactive labeling technique in a solution of 0.1 M $HClO_4$ + 5x10^{-4} M urea. The simulation results were obtained under condition specified in the upper left corner.

nitrogen is not chemisorbed on platinum at room temperature, the Auger electron data provide evidence that urea does not decompose on platinum upon system evacuation (and before). These observations are consistent with a picture in which the voltammetric peak observed with urea is associated with a phase transition between a Pt(100)c(2 x 4) submonolayer of urea with a coverage of approximately 1/4 on the positive-potential side of the peak and a Pt(100)(1 x 1) monolayer of H on the negative side. The broad voltammetric maxima observed in the urea-free case we interpret as being due to the supercritical passage between a H-free surface in the positive region and a monolayer of H in the negative region, through an intermediate-potential region with H coverage of approximately 1/2.

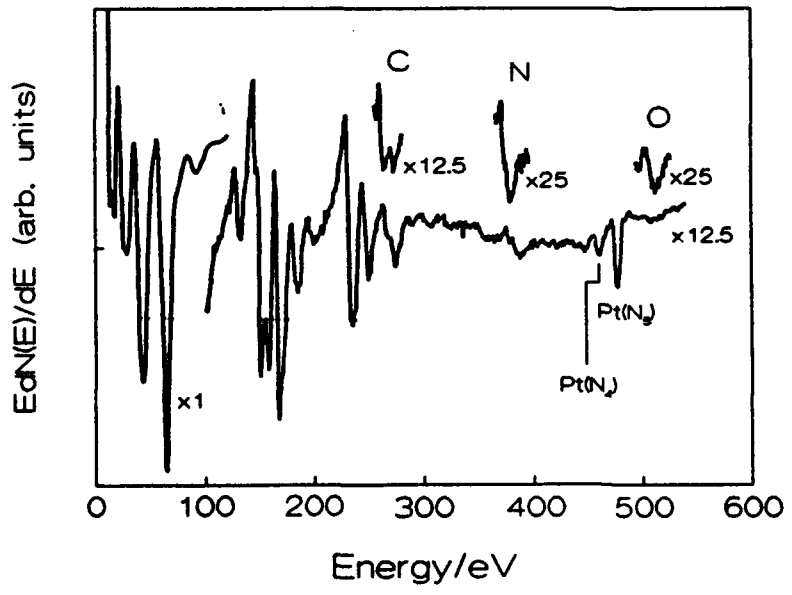

Figure 30. Auger electron spectra of the Pt(100) surface after adsorption in 10^{-3} M urea + 5x10^{-4} M H_2SO_4 at electrode potential -0.06 V. Beam energy 800 eV.

To account for the experimental observations we have developed a lattice-gas model based [60] on the assumption that urea

coordinates platinum surfaces through its nitrogen atoms. The Pt(100) surface is considered as a square lattice on which H can be adsorbed at the nodes and urea on the bonds. Simultaneous occupation by urea of two bonds that share a node is excluded, as is occupation by H of a node adjacent to a bond occupied by urea. The energies of the allowed configurations are described by a standard effective lattice-gas Hamiltonian The model is illustrated in Figure 31. How the modeling fits the experimental data is shown in Figure 29.

The effective interactions used in this work, which are given in the caption of Figure 31. In particular, the repulsive interactions between urea on neigh-boring rows of the Pt lattice, $\Phi_{UU}^{(1)}$, $\Phi_{UU}^{(2)}$, $\Phi_{UU}^{(4)}$ and $\Phi_{UU}^{(8)}$ limit the urea coverage to near 1/4 in the experimental range of electrode potentials and urea concentrations, and the weakly attractive $\Phi_{UU}^{(7)}$ selects c(2x4) configurations over those with (2x2) symmetry. The repulsive $\Phi_{UU}^{(3)}$ and $\Phi_{UU}^{(6)}$ between nearby urea molecules which point in mutually perpendicular directions govern the density of antiphase boundaries. The repulsive interactions between urea and nearby H, $\Phi_{HU}^{(1)}$ and $\Phi_{HU}^{(2)}$ limit the coverage of interstitial H in the c(2x4) phase. Their values significantly affect the detailed shapes of the simulated voltammograms. The weakly repulsive interaction between H on nearest-neighbor sites, $\Phi_{HH}^{(1)}$, was adjusted to match the width of the simulated urea-free voltammogram to the experiments reported in ref. 39.

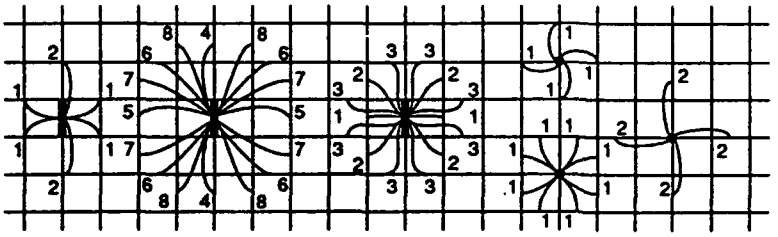

Figure 31. The square Pt(100) lattice with adsorbed urea (bars) and H (circles). The effective pair interactions are denoted by numbered curves. Nearest-neighbor sites are connected by $\Phi_{HH}^{(1)}$; urea and H by $\Phi_{HU}^{(i)}$, i = 1,2; and urea molecules by $\Phi_{UU}^{(i)}$, i = 1,...,8. In the simulations presented here we used (in kJ mol^{-1}): $\Phi_{HH}^{(1)}$ = -2.0, $\Phi_{HU}^{(1)}$ = -8.0, $\Phi_{HU}^{(2)}$ = -4.0, $\Phi_{UU}^{(1)}$ = -13.0, $\Phi_{UU}^{(2)}$ = -10.0, $\Phi_{UU}^{(3)}$ = -6.0, $\Phi_{UU}^{(4)}$ = -0.5, $\Phi_{UU}^{(5)}$ = -2.5, $\Phi_{UU}^{(6)}$ = -3.0, $\Phi_{UU}^{(7)}$ = +0.25 and $\Phi_{UU}^{(8)}$ = -2.0.

We have reported a complete experimental and theoretical description of urea adsorption on the Pt(100) electrode. We have used voltammetry, radiochemistry, LEED and quantitative Auger electron spectroscopy, as well as Monte Carlo simulations of a

new lattice-gas model developed for this study, and demonstrated that the simulation results agree well with those of our experiments. These include an ordered c(2x4) adsorbed urea phase and sharply peaked voltammograms. We interpret our observations as associated with a phase transition between the urea phase for potentials on the positive side of the peak and a (1x1) monolayer of hydrogen phase on the negative side. The main products of this research are the lattice-gas model which describes the microscopic adsorption geometry and the effective lateral interaction energies of the urea surface species involved in the phase transition behavior.

IV. CONCLUSIONS

Methodology. The radiochemical technique developed at Urbana for studying single-crystal/solution interfaces has proven to be a direct and reliable source of information in in situ surface electrochemistry. The radiochemical data have been complemented by results obtained the ultra-high vacuum characterization of emersed electrodes. The success of such a comparative program hinged on the relevance of the vacuum approach in investigations of the reversible adsorbates. A noticeable fraction of the time in the AFOSR supported program was devoted to provide evidence that the vacuum approach is a relevant analytical technique of surface electrochemistry. As usual with all other physical techniques in the solid/liquid research, it has its pros and contras. Therefore, a multitechnique approach is needed to characterize the solid/liquid interface on the molecular level. The parallel application of the in situ and ex situ techniques, and electrochemistry, practiced in this program was meant to conform to this multitechnique research strategy.

Structure/function relationship in methanol catalysis. The rates of catalytic electrooxidation of methanol vitally depend on the choice of surface geometry of platinum electrodes. Using chronoamperometry, we have found that the catalytic oxidation rate increase by a factor of 50 when the Pt(110) electrode is used as compared to the Pt(111) electrode. We have provided evidence that adsorbed bisulfate significantly retards the methanol oxidation processes. Therefore, we conclude the *function* of anions in the type of catalysis studied in this project is to inhibit the electrocatalytic rates. As an example of our focus on the *structure*, we have shown that the adsorbed bisulfate creates well-ordered ($\sqrt{3}x\sqrt{3}$) adlattices on Pt(111). The perfection of the "$\sqrt{3}$" structure of the closed-packed bisulfate adlayer is related to the symmetry match of the bisulfate oxygens and the hexagonal symmetry of the (111) plane of platinum. Also, a clear trend has been identified with respect to the order of adsorption strength on the single crystal electrodes studies: Rh(111) > Rh(100) > Pt(111) ≈ Au(111) > Pt(100). For platinum, this correlates well with the inhibition trend in the methanol oxidation kinetics. We have concluded that the (bi)sulfate interactions with metal electrodes is not purely electrostatic, there is chemical bonding component that increases in significance in the series: perchlorate, (bi)sulfate and phosphate. Finally, we have documented an enhanced adsorption in all the systems studied (that is, more anions are adsorbed along with the metal underpotential deposition). Since the anions inhibit methanol electrolysis, the anticipated catalytic enhancement by the metal

adatoms will be counteracted by the inhibition through the excessively adsorbed anions. This observation should be taken into account in modeling more advanced, multicomponent electrocatalysts in future catalytic electrochemical technologies.

Anion adsorption on clean substrates. We have also investigated some other features of anionic adsorption that are related to a broader understanding of the structure of the solid/liquid interface, rather than to catalysis. We have been able to provide a complete, or near-complete, description of the bisulfate adsorption on several crystallographic planes of platinum, rhodium and gold at a constant temperature. In addition to quantifying adsorption by the radiochemistry and Auger electron spectroscopy, and reporting on the adsorption isotherms, we have addressed such issues as the deficiency of bisulfate adsorption on the Pt(100) electrode, and on the origin of the "unusual" splitting of the Pt(111) and Au(111) voltammetry. We have proposed that some form of water discharge accounts for the desorption of bisulfate from the Pt(100) electrode with the increase in the positive charge of the electrode. Concerning the adsorption of bisulfate on the Pt(111) and Au(111) electrodes, we have shown that the number of electrons formally exchanged per one adsorbed anion is close to two. One may conclude that the electric charge measured, and the related voltammetric profiles, originate from the divalent sulfate adsorption. However, some of our work, and the numerous studies by other investigators, have considered the formation of a high-energy-hydrogen as a principal cause of the voltammetric splitting in the traditional double layer range of the Pt(111) electrode. It is realistic to assume that the unusual voltammetric current observed with the Pt(111) and Au(111) electrodes may be of different origin. The search for a conclusive solution should probably be postponed until new methods of surface imaging become available. We have also provided evidence that voltammetric properties of the polycrystalline platinum electrode give an indication of a superposition of the adsorbates that have their individual Γ vs. E characteristics associated with the different crystallographic facets of the surface.

Perchlorate reduction. Perchlorate reduction, that is a strong anion-surface interaction, has been demonstrated on the rhodium electrodes. We conclude that unlike most noble metals which are barely active in the perchlorate reduction, rhodium appears to have electronic configuration that facilitates an efficient surface reduction to chloride. The Rh(100) orientation has the most appropriate surface geometry to perform the reductive heterogeneous catalysis.

Adsorption of anions on thin metallic films. The challenge for the work with ultra-thin metallic films has been to measure the electrode potential dependency of the adsorbed anions and to relate such a dependency to current-potential profiles due to the deposits formation. The analysis of the electric current data and the radiochemical results have demonstrated the principles of *enhanced adsorption* using cadmium, copper and silver as ultra thin metallic films. We have shown, for the first time, that there are active and inactive metal adlayers with respect to bisulfate adsorption. The cadmium UPD film created at the most positive potentials is apparently composed of some oxides or hydroxides of this metal. With copper electrodeposited on the Pt(111) electrode, we conclude that a replacement of bisulfate by perchlorate occurs. Notably, the formation of

the UPD oxidized phase was not observed in our studies of neither *silver nor copper deposition on gold.* Evidently, the Pt/Cu multicomponent electrode has a stronger affinity to perchlorate than, for instance, has the Au/Cu electrode. This has allowed us to conclude that the support properties have a major effect on the chemical properties of the deposited films of the monolayer dimensions. We have also observed that sliver electrodissolution from the platinum (111) electrode is interrupted by the oxide Ag/Pt formation that significantly affects bisulfate adsorption on the Pt/Ag substrate. We have also investigated palladium monolayers on the Pt(111) substrates and the deposition of silver on the Rh(111) electrode. These initial studies open new avenues of research in surface electrochemistry for the P.I. laboratory.

Studies in CO poisoning. The experimental evidence reported by many authors designate surface CO as the methanol chemisorption products. The current understanding is that the products are most likely composed of a mixed population of the linear and bridge bonded CO molecules. We have studied the solid/liquid CO by the use of techniques of ultra-high vacuum surface science and electrochemistry on the Pt(111), Rh(111) and Pt(100 electrodes. The LEED data corresponding to the CO saturation coverage give the surface structures of ($\sqrt{3}$ x 3)rect., split(2x2) and c(4x2), respectively. **These are the same structures as found in the earlier gas phase studies of the equivalent surface systems.** When lower CO coverage was produced on platinum, we have seen the CO islands possessing internal organization of these high-packing structures. However, the stability of such islands is limited and a slow structural rearrangement of the Pt(111)($\sqrt{3}$ x 3)rect to a Pt(111)c(4 x 2) surface structure occurs. For the Pt(100) surface, we have obtained a complete Auger electron spectroscopy characterization of the electrochemical CO adsorbate. In this case, the data closely correspond to the previously reported spectral features for carbon monoxide adsorbed on several relevant catalytic substrates in the gas phase. These finding document a close relationship between species involved in gas phase and solution phase surface science and, indirectly, between heterogeneous catalysis and electrocatalysis.

Phase transitions with urea adsorbed on the Pt(100) electrode. The voltammetry for the Pt(100) electrode in solution containing urea is unique and has motivated us to develop a proper formalism to interpret it. In a collaboration with Professor P. A. Rikvold, FSU, we have developed a lattice-gas model based on assumption that urea coordinates platinum surfaces through its nitrogen atoms. We demonstrate that the simulation results agree well with those of our experiments. We interpret our observations as associated with a phase transition between the urea phase for potentials on the positive side of the peak and a (1x1) monolayer of hydrogen phase on the negative side, and provide the effective lateral interaction energies of the urea surface species involved in the phase transition behavior.

In brief, *by combining data from electrochemistry, radiochemistry and from the LEED/Auger/XPS/UHV spectroscopies, we have developed surface chemistry of the reversible adsorbates on the single crystal electrodes and the metallic ultra-thin films. Since most of the surfaces investigated display distinctive electrocatalytic properties, and the reversibly adsorbed constituents are always*

present in practical electrolytes, this study has provided vital information on the role of the electrochemical environment in electrocatalysis. Specifically, we have shown how important is a deliberate tailoring of the composition of the solid/liquid interface -- with respect to the studied anions -- in methanol oxidation kinetics on platinum. Our research objective also was to outline the significance of atomic-level structural and electronic factors in the organization of the studied solid-liquid interfaces, and to connect concepts in surface electrochemistry with those in gas phase surface science. This latter connection has been particularly well documented with respect to CO poisoning. In the latest phase of this research we have focused on the consolidation of all pieces of information obtained over the four years of study. In addition to this report, some of the data and the derived generalization contained in this report, will be presented in a review article that is prepared for publication [37].

V. CUMULATIVE LIST OF PUBLICATIONS ACKNOWLEDGING AFOSR SUPPORT

Published:

1. A. Wieckowski, Interim Reports for AFOSR (5/1990 - 4/1993) "Ionic and Molecular Environments in Heterogeneous Electrocatalysis: Studies by Radioactive Labeling and LEED/Auger Spectroscopy".

2. E. K. Krauskopf and A. Wieckowski, J. Electroanal. Chem., 271, 295 (1989). "Acetic Acid Adsorption on Smooth Pt Electrodes: Measuring the Rate of Double-Layer Organization and Rearrangement".

3. E. K. Krauskopf, L. M. Rice-Jackson and A. Wieckowski, Langmuir, 6, 970 (1990). "Pyridine Adsorption on Polycrystalline Platinum Studied by the Radioactive Labeling Method".

4. M. Hourani, M. Wasberg, C. Rhee and A. Wieckowski, Croat. Chem. Acta, 63, 373 (1990). "Contrasting Surface Behavior of Rh(111) and Pt(111) Electrodes".

5. M. Wasberg, M. Hourani and A. Wieckowski, J. Electroanal. Chem., 278, 425 (1990). "Comparison of Voltammetry of Vacuum-Prepared Rh(100) and Rh(111) Electrodes".

6. P. Zelenay, L. M. Rice-Jackson and A. Wieckowski, J. Electroanal. Chem., 283, 389 (1990). "Radioactive Labeling Study of Sulfate/Bisulfate Adsorption on Smooth Gold Electrodes".

7. P. Zelenay, L. M. Rice-Jackson and A. Wieckowski, Langmuir, 6, 974 (1990). "Adsorption of Pyridine on Polycrystalline Gold Electrode Studied by Radioactive-Labeling Method".

8. D. Zurawski, M. Wasberg and A. Wieckowski, J. Phys. Chem., 94, 2076 (1990). "Low-Energy Electron Diffraction and Voltammetry of Carbon Monoxide Electrosorbed on Pt(111)".

9. C. K. Rhee, M. Wasberg, G. Horanyi and A. Wieckowski, J. Electroanal. Chem., 291, 281 (1990). "Strong Anion/Surface Interaction: Perchlorate Reduction on the Rh(100) Electrode Studied by Voltammetry".

10. G. Horányi and A. Wieckowski, J. Electroanal. Chem., 294, 267 (1990). "Radiotracer Study of Adsorption of HSO_4^- Ions Induced by Cd^{2+} Adatoms at a Smooth Polycrystalline Platinum Electrode".

11. E. K. Krauskopf and A. Wieckowski, J. Electroanal. Chem., 296, 159 (1990). "Molecular Orientation of Hydroquinone on Smooth Platinum Electrodes Studied by Radioactive Labeling".

12. A. Wieckowski, in: J. O'M. Bockris, B. E. Conway, and R. E. White (Eds.), Modern Aspects of Electrochemistry, "In Situ Surface Electrochemistry: Radioactive Labeling", Vol. 21, Plenum Press, New York, 1990 (review article).

13. P. Zelenay, G. Horanyi, C. K. Rhee and A. Wieckowski, J. Electroanal. Chem., 300, 499 (1991). "Voltammetric and Radioactive Labeling Studies of Single Crystal and Polycrystalline Rhodium Electrodes in Sulfate-Containing Electrolytes".

14. P. Zelenay and A. Wieckowski, in: H. D. Abruña (Ed.), Electrochemical Interfaces: Modern Techniques for In-Situ Surface Characterization, "Radioactive Labeling: Towards Characterization of Well-Defined Surfaces", VCH Publishers, New York, 1991 (review article).

15. M. Rubel, C. K. Rhee, A. Wieckowski and P. A. Rikvold, J. Electroanal. Chem., 315, 301 (1991). "Cyclic Voltammetry of Platinum Single Crystal Electrodes in Solutions Containing Urea".

16. A. Wieckowski, P. Zelenay and K. Varga, J. Chim. Phys., 88, 1247 (1991). "A Comprehensive Study of Bisulfate Adsorption on Pt(111) by Radioactive Labeling and Voltammetry".

17. P. Zelenay, L. M. Rice-Jackson, J. Gawlowski and A. Wieckowski, Surf. Sci., 256, 253 (1991). "Radioactive Labeling Study of Bisulfate Adsorption on Copper Adatoms Deposited on the Gold Electrode in Neutral Media".

18. C. K. Rhee, M. Wasberg, P. Zelenay and A. Wieckowski, Catalysis Letters., 10, 149 (1991). "Reduction of Perchlorate on Rhodium and its Specificity to Surface Crystallographic Orientation".

19. E. K. Krauskopf and A. Wieckowski, in Frontiers of Electrochemistry, "Radiochemical Methods to Measure Adsorption at Smooth Polycrystalline and Single Crystal Surfaces" P. N. Ross and J. Lipkowski (eds.), VCH Publishers, NY, New York, 1992.

20. K. Varga, P. Zelenay and A. Wieckowski, "J. Electroanal. Chem., 327, 291 (1992). "Adsorption Anions on Ultra-Thin Metal Deposits on Single Crystal Electrodes. Part I. Voltammetric and Radiochemical Study of Bisulfate Adsorption on Pt(111) Electrodes Containing Cadmium Adatoms.

21. K. Varga, P. Zelenay and A. Wieckowski, J. Electroanal. Chem., 330, 453 (1992). "Adsorption of Anions on Ultra-Thin Metal Deposits on Single Crystal Electrodes. Part II. Voltammetric and Radiochemical Study of Bisulfate Adsorption on Pt(111) and Pt(poly) Electrodes Containing Copper Adatoms".

22. P. A. Rikvold and A. Wieckowski, Physica Scripta, , T44, 71 (1992). Some "Applications of Lattice-Gas Models to Electrochemical Adsorption".

23. J. Weaver, S.-C. Chang, L.-W. H. Leung, X. Jiang, M. Rubel, M. Szklarczyk, D. Zurawski and A. Wieckowski, J. Electroanal. Chem., 327, 247 (1992). "Evaluation of Absolute Saturation Coverages of Carbon Monoxide on Ordered Low-Index Platinum and Rhodium Electrodes".

24. Zelenay and A. Wieckowski, J. Electrochem. Soc. 139, 2552 (1992), "Radiochemical Assay of Adsorption at Single Crystal/Solution Interfaces".

25. D. Zurawski and A. Wieckowski, Langmuir, 8, 2313 (1992). "Lateral Modification and Organization of CO-I Mixed Adlattices on Pt(111)".

26. M. Gamboa-Aldeco, E. Herrero, P. Zelenay and A. Wieckowski, J. Electroanal. Chem., 348, 451 (1993). "Adsorption of Bisulfate Anion on the Pt(100) Electrode. The Comparison with Pt(111) and Pt(poly).

Accepted for publication:

27. P. Zelenay, M. Gamboa-Aldeco and A. Wieckowski, J. Electroanal. Chem., "Adsorption of Anions on Ultra-Thin Metal Deposits on Single Crystal Electrodes. Part III. Voltammetric and Radiochemical Study of Bisulfate Adsorption on Pt(111) and Pt(poly) Electrodes Containing Silver Adatoms", in press.

28. A. Wieckowski, J. Electroanal. Chem., Comments on "In Situ Studies of Organic Compounds on Platinum Electrodes" by J.O'M Bockris and K. T. Jeng.

29. J. Lipkowski, L. Stolberg, S. Morin, D.E. Irish, P. Zelenay, M. Gamboa-Aldeco and A. Wieckowski, J. Electroanal. Chem., "Probing Pyridine Adsorbed at Gold Electrodes by Chronocoulometry, Radiochemistry and Raman Spectroscopy".

30. C. K. Rhee, J. Feliu, E. Herrero, P. Mrozek and A. Wieckowski, J. Phys. Chem., "Auger Electron Spectroscopy, Low-energy Electron Diffraction and Voltammetry of Carbon Monoxide on a Pt(100) Electrode".

31. M. Han, P. Mrozek and A. Wieckowski, Phys. Rev. B, "XPS and AES Study of Ultra-Thin Palladium Films on Pt(111) Substrate".

32. Z. Shi, J. Lipkowski, M. Gamboa, P. Zelenay and A. Wieckowski, J. Electroanal. Chem. "Investigations of SO_4^{2-} adsorption at Au(111) Electrode by Chronocoulometry and Radiochemistry",

33. P. A. Rikvold, A. Wieckowski, Q. Wang, C. K. Rhee, and M. Gamboa in Computer Simulation Studies in Condensed Matter Physics VI, edited by D. P. Landau, K. K. Mon, and H. B. Schattler (Springer, Heidelberg), "Monte Carlo Simulation of Urea Adsorption on Platinum".

Submitted:

34. M. Gamboa-Aldeco, K. Franaszczuk and A. Wieckowski, CRC Press, "Radiotracer Study of Electrode Surfaces".

In preparation:

35. P. Mrozek, C. K, Rhee, M. Han and A. Wieckowski, J. Phys. Chem., "Auger

Electron Spectroscopy, Ionization Loss Spectroscopy and Cyclic Voltammetry of Bisulfate Adsorption on Pt(111)".

36. E. Herrero, K. Franaszczuk, M. Gamboa-Aldeco, P. Mrozek and A. Wieckowski, Science, "Marcusian Treatment of Anionic Effects in Methanol Oxidation Kinetics on the Platinum (111) Electrode".

37. A. Wieckowski, Invited review article for Critical Review in Surface Science, M. A. Sherwood (ed). "Ultra-High Vacuum Surface Science with Single Crystal Electrodes: Relevance and Significance". .

38. P. Mrozek, M. Han, M. Gamboa-Aldeco and A. Wieckowski, J. Phys. Chem., "Auger Electron Spectroscopy, Radiochemistry and Cyclic Voltammetry of Bisulfate Adsorption on the Clean and Silver Covered Au(111) Electrode".

39. M. Gamboa, P. Mrozek, C. P. Rhee, Qing Wang, A. Wieckowski, and P. A. Rikvold", Surf. Sci., "Adsorption of Urea on the Pt(100) Electrode: Experiments and Lattice-Gas Modeling".

Other key references:

40. K. Fanaszczuk, E. Herrero, P. Zelenay, A. Wieckowski, J. Wang and R. I. Masel, J. Phys. Chem., 96, 8508, 1992.

41. A. Wieckowski's presentations:

181st Meeting of The Electrochemical Society, St. Louis, Missouri, May 17-22, 1992. "Potential Step and NMR Investigations of the Oxidation and Adsorption of Methanol on Platinum Surfaces".

183rd Meeting of The Electrochemical Society, Honolulu, Hawaii, May 16-21, 1993. "Catalytic Decomposition of Methanol on Platinum Single Crystal Electrodes: An Endless Subject of Desire".

42. R. Parsons and T. VanderNoot, J. Electroanal. Chem., 257, 9 (1988), and references therein.

43. P. J. Slezak and A. Wieckowski, J. Mag. Reson., A 102, 166 (1993)

44. L. H. Leung, T. W. Gregg and D. W. Goodman, Langmuir, 7, 3205 (1991), and references therein.

45. C. Ammer, Phys. Stat. Sol. (a) 71, 135-145 (1982) parts I and II

46. C. H. Chen, S. M. Vesecky and A. A. Gewirth, J. Am. Chem. Soc., 141, 451 (1992)

47. N. Kimizuka and K. Itaya, Faraday Discuss., 94 (1993), in press

48. J. McBreen, W. E. O'Grady, G. Tourillon, E. Dartyge and A. Fontaine, J. Electroanal. Chem., 307, 229 (1991)

49. J. L. Stickney, S. D. Rosasco, D. Song, M. P. Soriaga and A. T. Hubbard, Surface Sci., 130, 326 (1983), and other Hubbard's papers on this topic.

50. N. C. Gibson, P. M. Saville and D. A. Harrington, J. Electroanal. Chem., 318, 271 (1991)

51. G. K. Wertheim and P. H. Citrin, in Photoemission in Solids, part I, M. Cardona and L. Ley, eds., Springer, Berlin, 1978, p. 197.

52. E. Stuve, private communication

53. W. Wurth, P. Feulner and D. Menzel, Physica Scr. T41, 213 (1992).

54. E. Umbach and Z. Hussein, Z. Phys. Rev. Lett. 52, 457 (1984).

55. J. P. Biberian and M. A. Van Hove, M. A. Surface Sci., 118, 443 (1982).

56. S. C. Chang and M. J. Weaver, J. Phys. Chem. , 94, 5095 (1990).

57. R. J. Behm, P. A. Thiel, P. R. Norton and G. J. Ertl, J. Chem. Phys., 78, 7437 (1983).

58. A. Wieckowski, Electrochim. Acta, 26, 1121 (1981).

59. G. Horanyi, G. Inzelt and E. M. Rizmayer, J. Electroanal. Chem., 98, 105 (1979).

60. P. A. Rikvold, Electrochim. Acta 36 (1991) 180 and references cited therein.